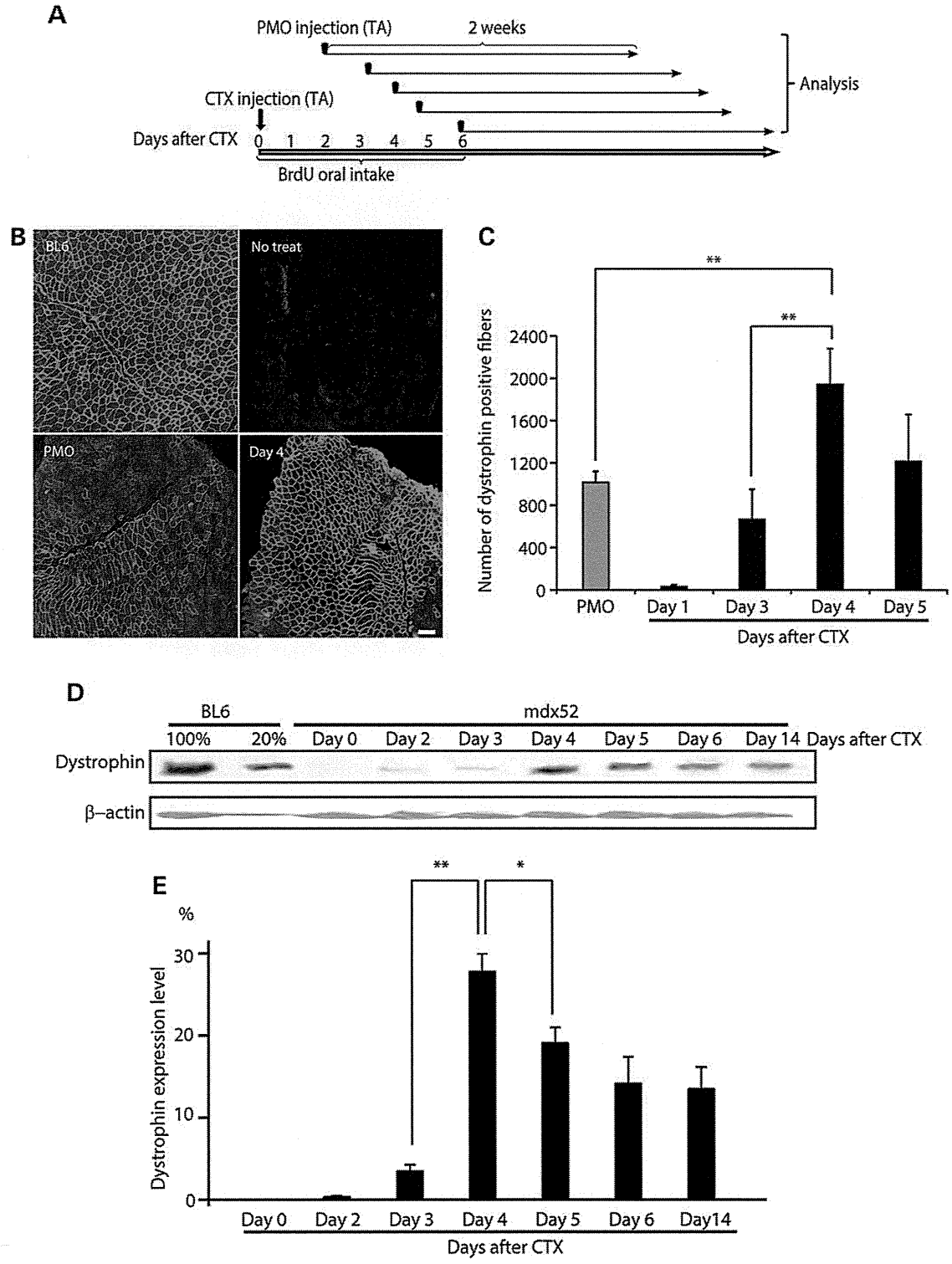

Figure 3. Evaluation of PMO entry into regenerating fibers during synchronized regeneration due to CTX injection in *mdx*52 mice. (A) Experimental model of the local intramuscular injection of CTX or PMO into *mdx*52 mice. Day 0 is defined as 5 weeks of *mdx*52 mice. CTX was injected into the TA muscles of *mdx*52 mice at Day 0. Between Day 0 and Day 6, PMO (400 μg/kg body weight) was injected into the CTX-injured TA muscles of *mdx*52 mice with oral administration of BrdU containing water (0.8 mg/ml). Analysis was performed 2 weeks after the PMO injection. (B) Immunohistochemical staining for dystrophin in the cryosections in TA muscles of *mdx*52 mice. Data are representative of six independent experiments. BL6: TA muscle from a WT C57/BL6. No treat: Untreated TA muscle from *mdx*52 mice. PMO: PMO-treated TA muscle from *mdx*52 mice. Day 4: PMO-treated CTX-injured TA muscle from *mdx*52 mice (CTX was injected 4 days before the PMO injection). Scale bar, 100 μm. (C) Percentage of dystrophin-positive fibers in CTX-injured TA muscle. The data ($n = 6$) are presented as mean ± SD. $^{**}P < 0.01$. (D) Western blotting for dystrophin in the CTX-injured TA muscles of *mdx*52 mice. Data are representative of four independent experiments. BL6 20%: TA muscle from a 20% extract of WT C57/BL6 mice. Anti-β-actin is used as loading controls. (E) Semi-quantitative analysis of dystrophin expression in TA muscles of *mdx*52 mice 2 weeks after the intramuscular injection of PMO. The data ($n = 4$) are presented as mean ± SD. $^{*}P < 0.05$ and $^{**}P < 0.01$.

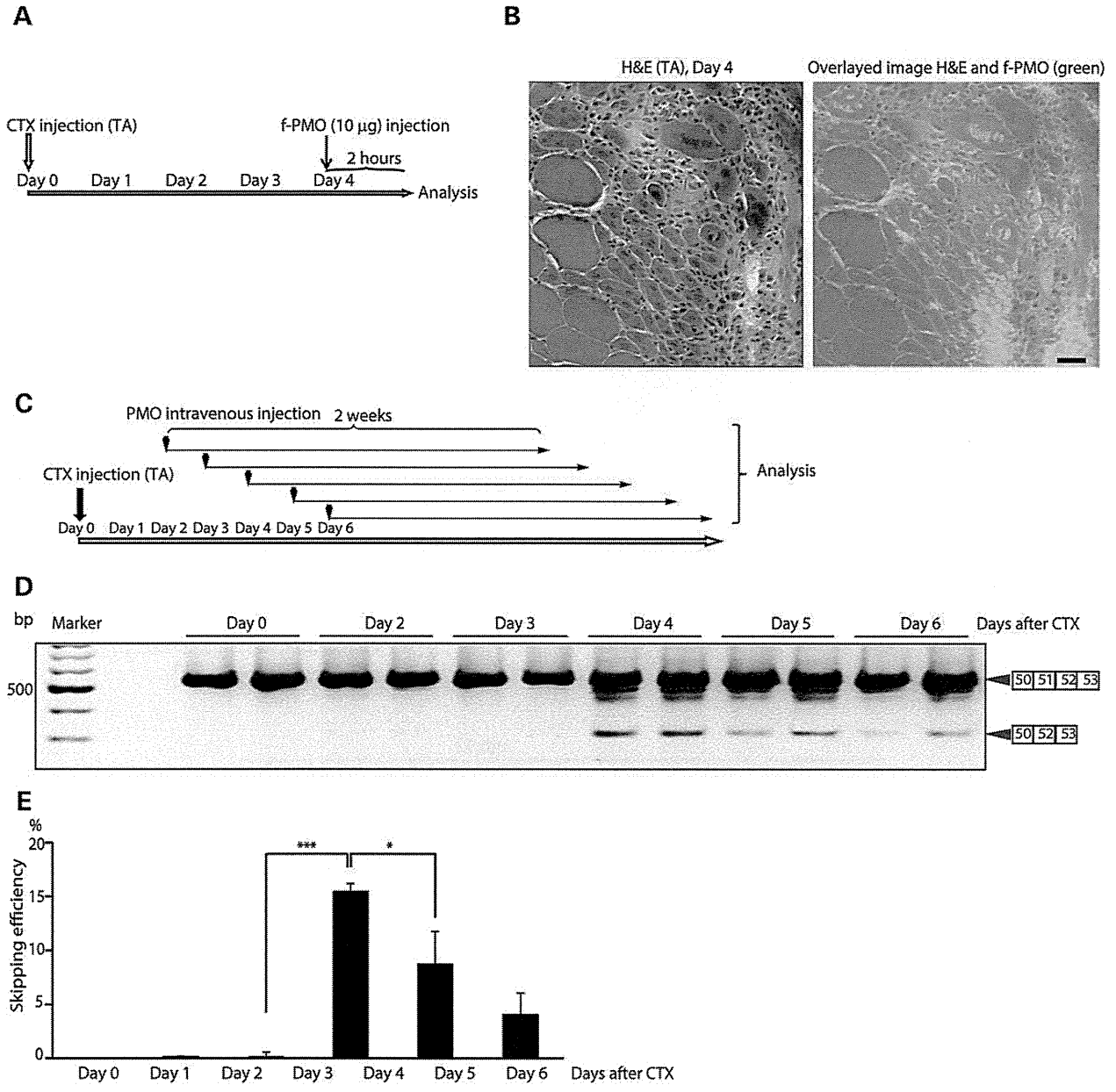

Figure 4. Skipping efficiency is increased dramatically when PMO is injected systemically at 4 days after CTX injury in WT mice. (A) Experimental model of the intramuscular injection of f-PMO into BL6 WT mice. f-PMO (400 μg/kg body weight) was injected into the CTX-injured TA muscles of *mdx*52 mice at Day 4 and the TA muscles analyzed 2 h after the injection of f-PMO. (B) Hematoxylin and eosin (H&E) staining (left) and immunofluorescence imaging of injured TA muscle for the detection of f-PMO (right). (C) Experimental model of the systemic intravenous injection of PMO into WT mice. Day 0 is defined as 5 weeks of WT mice. CTX was injected into the TA muscles of WT mice at Day 0. Between Day 0 and Day 6, PMO (320 mg/kg) was injected intravenously via tail vein into WT mice that had already received a CTX injection into TA muscles. RT–PCR analysis was performed 2 weeks after the PMO injection, respectively. (D) Detection of exon 51-skipped dystrophin mRNA by RT–PCR. Data are representative of four independent experiments. (E) Quantitative analysis by RT–PCR of exon 51 skipping by PMO. The percentages of skipped bands in each lane of (E) are shown. The data ($n = 4$) are presented as mean ± SD. $^{*}P < 0.05$ and $^{***}P < 0.001$.

muscles of 5-week-old WT mice, followed, 4 days later, by injection of f-PMO (400 μg/kg body weight) targeting the splice donor site of exon 51 into each TA muscle (Fig. 4A). Two hours later, the mice were killed and TA muscles were removed for microscopic analysis. Clearly, 4 days after CTX injection f-PMO had entered small-caliber-regenerated fibers of less than 35 μm, but not normal-caliber fibers with peripheral nuclei (Fig. 4B). Next, PMO 51Do (320 mg/kg) targeting the splice donor site of exon 51 was injected into the tail vein of 5-week WT mice 4 days after injection of CTX into their TA muscles (Fig. 4C). The mice were killed 2 weeks later and TA muscles were removed and analyzed by RT–PCR. The skipping ratios as evaluated by RT–PCR were 0.1, 0.3, 0.7, 15.3, 8.9 and 4.3% at Days 1, 2, 3, 4, 5 and 6 after the CTX injection,

respectively (Fig. 4D and E). These data show that small-caliber-regenerated fibers can take up PMO efficiently in WT mice with a strong preference at Days 4 and 5, the period of maximum myotube formation.

Efficient uptake of PMO by dystrophin-positive WT regenerated fibers at 4 days after CTX injection

We next analyzed the characteristics of eMHC-positive regenerated fibers induced by CTX injury (Fig. 5A). Four days after CTX intramuscular injection into TA muscles of 5-week-old WT mice, PMO 51Do (320 mg/kg) was injected via the tail vein. One hour later, the mice were killed and the TA muscles were removed for analysis by *in situ* hybridization with digoxigenin–alkaline phosphatase probes. This revealed that PMO 51Do was mainly present in the nucleus and to a lesser extent in the cytosol of small-caliber (<35 μm)-regenerated fibers, but was barely detectable in normal-caliber fibers with peripheral nuclei (Fig. 5B and C). Immunohistochemistry showed that fibers in which PMO 51Do was detected expressed dystrophin at the membrane (Fig. 5D and E).

In vitro evaluation of the period of uptake of PMO and 2′OMePS by mouse C2C12 myotubes

To examine the period of PMO uptake, we initially evaluated the expression level of dystrophin during C2C12 myoblasts differentiation and found the expression of dystrophin 24 h after the change of growth medium to differentiation medium by RT–PCR (Fig. 6A). Then, we transduced C2C12 myotubes with 10 μM PMO 51Do at 24, 48, 168 or 336 h after the medium change. We also tested the uptake period of 1 μM 2′OMePS, which is one of the commonly investigated oligonucleotides chemistries used for targeting the intraexonic site of exon 51. Undifferentiated C2C12 myoblasts after 10 μM PMO or 1 μM 2′OMePS were used as controls. After 48 h of incubation with PMO or 2′OMePS, the cells were collected and analyzed by RT–PCR (Fig. 6B and C). The skipping ratios of C2C12 myotubes after 10 μM PMO transfection were 32.6, 22.7, 9.8 and 6.1% after 24, 48, 168 or 336 h following the medium change, respectively (Fig. 6D). The skipping ratios after 1 μM 2′OMePS transfection over the same set of time periods were 22.9, 13.1, 2.5 or 1.2% after 24, 48, 168 or 336 h after the medium change, respectively (Fig. 6E). On the other hand, the skipping ratios of undifferentiated C2C12 myoblasts after 10 μM PMO or 1 μM 2′OMePS were 6.1 or 1.7%, respectively (Fig. 6D and E). These data support the idea that PMO or 2′OMePS is most efficiently taken up into muscle cells in the early stages of C2C12 myotube formation.

Proof of efficient PMO uptake by severely affected myofibers in dy^{3K}/dy^{3K} mice following systemic PMO injection

Finally, we performed PMO-mediated exon skipping for dy^{3K}/dy^{3K} mice, which are an animal model of laminin-α2 chain-deficient congenital muscular dystrophy and show severe dystrophic change with active muscle regeneration. Skipping exon 4 of the murine *Lama2* gene in dy^{3K}/dy^{3K} mice corrects the open reading frame and could lead to the production of a truncated laminin-α2 chain (Fig. 7A). We first identified effective AO sequences in dy^{3k}/dy^{3k} fibroblasts. We designed seven AO sequences targeting either exonic sequences or exon–intron junctions of the murine *Lama2* exon 4 (Fig. 7B; sequences in Table 3). We then transfected one or two of the seven AOs (10 μM in total) into dy^{3k}/dy^{3k} fibroblasts (17). After 48 h incubation, we analyzed RNA fractions by RT–PCR using the primers described in Supplementary Material, Figure S6. Among the AOs examined, PMO 4B plus 4D were shown to be capable of inducing exon 4 skipping at a level approaching 80%, the highest among the combinations that we examined by RT–PCR (Fig. 7C and D). 4B and 4D were designed to target the exonic sites of exon 4. We therefore injected the combination of two AOs (400 μg/kg body weight) into the TA muscles of dy^{3K}/dy^{3K} mice at age 10 days. Fifteen days later, TA muscles were obtained and analyzed by RT–PCR and immunohistochemistry. We found by RT–PCR that 4B plus 4D could induce exon 4 skipping (Fig. 8A). We confirmed correct exon 4 skipping by direct sequencing of the RT–PCR products (Fig. 8B). Moreover, up to 20% of fiber membranes were laminin-α2 positive by immunohistochemistry (Fig. 8C). After intraperitoneal injection (150 mg/kg in total) of the 2-PMO combination into dy^{3K}/dy^{3K} mice at postnatal at age 10 days, we found that 4B plus 4D could induce exon 4 skipping by RT–PCR (Fig. 8D). Our study results showed a trend toward improvement in life span of PMO-treated dy^{3k}/dy^{3k} mice compared with saline-treated dy^{3K}/dy^{3K} mice (Fig. 8E). These data suggest the potential of PMO-mediated therapy targeting myotubes for MDC1A.

DISCUSSION

We demonstrated here that PMO can be taken up into dystrophin and eMHC-positive regenerated fibers in WT mice. We also showed that PMO and 2′OMePS could be taken up into C2C12 myoblasts in the early stages of C2C12 myotube formation. These results suggest that we can apply PMO- or 2′OMePS-mediated therapy targeting myotube formation to other muscular diseases. To confirm our hypothesis, we finally showed the restoration of laminin-α2 chain expression by exon 4 skipping against the *Lama2* gene and a prolonged lifespan after intraperitoneal injection of PMO into dy^{3K}/dy^{3K} mice, which is a model of MDC1A (16).

PMO, which has a neutral chemistry, provides greatly decreasing the chance of catastrophic off-target antisense effects, and minimizes interactions with cationic moieties of proteins (11,18–21). These characteristics of PMO contribute to their extremely low toxicity and suitability for use in human. PMO is also being used extensively as a tool for selective inhibition of gene expression in cell culture models (22).

At present, the changes of membrane permeability of dystrophin-deficient muscle membrane, so-called 'leaky membrane hypothesis', facilitating a route of entry for the PMO into myofibers, are a favored explanation for PMO uptake (23–25). This hypothesis is based on the clinical evidence that dystrophin-deficient muscle fibers are prone to be injured by contraction and that the injury causes leakage of soluble cytoplasmic proteins such as creatine kinase (26,27). In addition, it is reported that intravenously delivered PMO shows very poor delivery to normal muscle, while dystrophin-deficient muscle

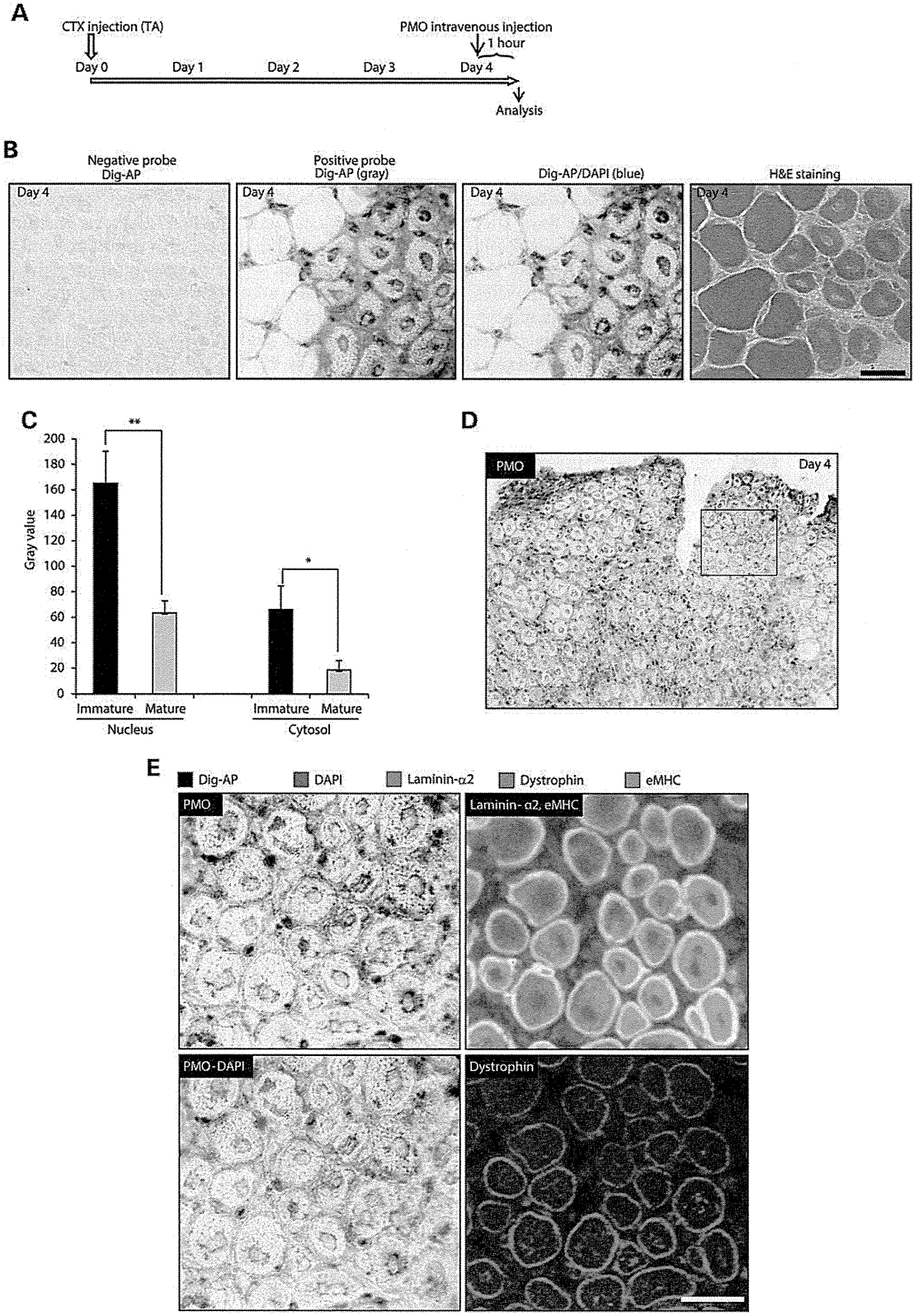

Figure 5. Detection of 25-mer PMO in myofibers on TA muscle cryosections by *in situ* hybridization. (A) Experimental model of the systemic intravenous injection of PMO into BL6 WT mice. Day 0 is defined as 5 weeks of WT mice. Cardiotoxin (CTX) was injected into the TA muscles of WT mice at Day 0. At Day 4, PMO (320 mg/kg) was injected intravenously via tail vein into the WT mice and TA muscles collected 1 h after the injection. (B) *In situ* hybridization for the direct detection of PMO

or intramuscular injection in normal muscle shows good delivery (28). Further, Evans blue, a low molecular-weight diazo dye which has a very high affinity for serum albumin, does not cross into skeletal muscle fibers in normal mice but *mdx* mice, a dystrophin-deficient animal model for DMD, show significant Evans blue accumulation in skeletal muscle fibers (29,30).

However, the hydrophobic plasma membrane constitutes an almost insurmountable barrier around muscle fibers, resulting in poor delivery of the neutral PMO, and preventing optimization of PMO-mediated therapy for DMD or other muscular dystrophies (31,32). To overcome this delivery issue with PMO, recent developments using cell-penetrating peptide-conjugated PMO, where a short cationic peptides that penetrate cells by interacting with the negatively charged plasma membrane, may become an effective strategy for reducing both dose levels and administration frequencies (33–36). But we still face issues of off-target effects or high toxicity in humans because of the nonspecific delivery-facilitated properties and the facilitated interactions with other proteins (37–40). Therefore, it is important to understand the detailed mechanisms of PMO entry into muscle fibers to improve the poor delivery of PMO and optimize it as a therapeutic intervention for DMD or other muscular diseases.

In this study, we found that exon 51 skipping was induced dose dependently in *mdx*52 mice but that no skipping was induced in WT mice after systemic injection of PMO (640 mg/kg). This finding conforms the 'leaky membrane hypothesis'. However, PMO was most efficiently taken up into eMHC-positive regenerating fibers at 4 days following CTX injection into TA muscles, which express dystrophin at the muscle plasma membrane in WT mice. The degeneration–regeneration process induced by CTX injection was well documented as follows: after CTX injection, satellite cell proliferation occurs within 2 days, myogenic differentiation is initiated within 3 days, new myotube formation is evident within 5 days and muscle architecture is largely restored within 10 days (41). Taken together, our *in vivo* study by CTX injection suggests PMO uptake is more prominent during stages from myogenic differentiation to myotube formation than cell proliferation stage. We also showed that PMO and 2′OMePS is taken up efficiently in the early stages of C2C12 myotube formation. These data suggest that the uptake mechanism is not simply attributable to a change in membrane permeability but also involves an unknown mechanism in the early stages of C2C12 myotube formation. It is reported that PMO internalization in uptake-permissive cells is specific, saturable and energy dependent, suggesting a receptor-mediated mechanism (22). These data suggest that immature regenerated fibers, which are called myotubes, could take up PMO more efficiently than mature fibers. In consequence, we confirmed that there is already a leaky gateway into dystrophin-deficient muscle fibers. But more importantly, these findings provide a conceptual advance in that it supports the idea that PMO entry into muscle fibers is dependent on a developmental stage in myogenesis rather than on an intrinsic defect in the dystrophin-deficient muscle membrane: the 'leaky-membrane' hypothesis. As such it provides a platform for developing PMO-mediated therapies for a variety of muscular disorders, such as MDC1A, that involve active muscle regeneration.

To test the potential of PMO treatment targeting myotube formation, we used the dy^{3K}/dy^{3K} mouse which is a model of MDC1A. The dy^{3K}/dy^{3K} mice, with a pMC1neo polyA+ cassette in exon 4 of the *Lama2* gene, are a null mutant for the laminin-α2 chain which is a major component of basal lamina in skeletal muscle and the peripheral nervous system (16). In man, the laminin-α2 chain consists of six domains (I–VI) and exon 4 of the *LAMA2* gene encodes a part of domain VI, which are predicted to form N-terminal globular (LN) structures (Supplementary Material, Fig. S7A) (42). The LN structures are essential for laminin aggregation into supramolecular networks and consequently for incorporation into basement membranes, thus mutations in this structures reduce the capacity of polymer formation (43). Another merosin-deficient mouse, the dy^{2J}/dy^{2J} mouse, harbors a mutation in the LN structures which leads only to slightly reduced expression of a laminin-α2 chain partially lacking these structures and thus displays a relatively mild muscular dystrophy and peripheral neuropathy (44). Therefore, we hypothesized that PMO-mediated exon 4 skipping could act to rescue dy^{3K}/dy^{3K} mice. In this study, we successfully confirmed the recovery of laminin-α2 chain by skipping of the mutated exon 4. Our data suggest that PMO, which was taken up into muscle fibers, may induce exon 4 skipping in dy^{3K}/dy^{3K} mice. More importantly, PMO-mediated exon 4 skipping has a real potential to become an effective therapy for MDC1A, since two nonsense mutations in exon 4 such as 547G > ANN166X and 677C > T/210X can cause MDC1A (45). Furthermore, half of the patients with congenital muscular dystrophy in European populations have mutations of the *LAMA2* gene (42), our data could offer a hope to patients struggling with the disease.

In conclusion, PMO or 2′OMePS is taken up preferentially into mouse muscle cells during myotube fusion. Our results can provide a platform for developing PMO-mediated therapies for a variety of muscular disorders, such as MDC1A, that involve active muscle regeneration. They also directs us to interrogate myogenic developmental mechanisms as opposed to defects in membrane function in mature muscle fibers for clues as to how to facilitate PMO delivery in other myopathies.

MATERIALS AND METHODS

Animals

Exon 52-deficient, X chromosome-linked muscular dystrophy (*mdx*52) mice were produced by a gene-targeting strategy and maintained at our facility (15). The mice have been backcrossed to the C57BL/6J WT strain for more than eight generations. Male *mdx*52 mice ages 3–32 weeks and WT mice age 5 weeks were used in this study.

on frozen TA muscle cryosections 1 h after systemic intravenous injection of the PMO into WT mice that had received CTX injection at Day 0; H&E, hematoxylin and eosin staining. (C) Quantitative analysis of the intensity of positive probe signal in muscle fibers 1 h after the PMO injection. The data ($n = 4$) are presented as mean ± SD. $^{*}P < 0.05$ and $^{***}P < 0.001$. (D and E) *In situ* hybridization for the direct detection of PMO on TA muscle cryosections. Data are representative of four independent experiments. (E) Enlarged view of rectangle area in (D). Staining of serial cryosections with anti-eMHC antibody (green), anti-laminin α2 chain antibody (pink), DAPI (blue) and anti-dystrophin antibody (red). Dig-AP: digoxigenin-alkaline phosphatase.

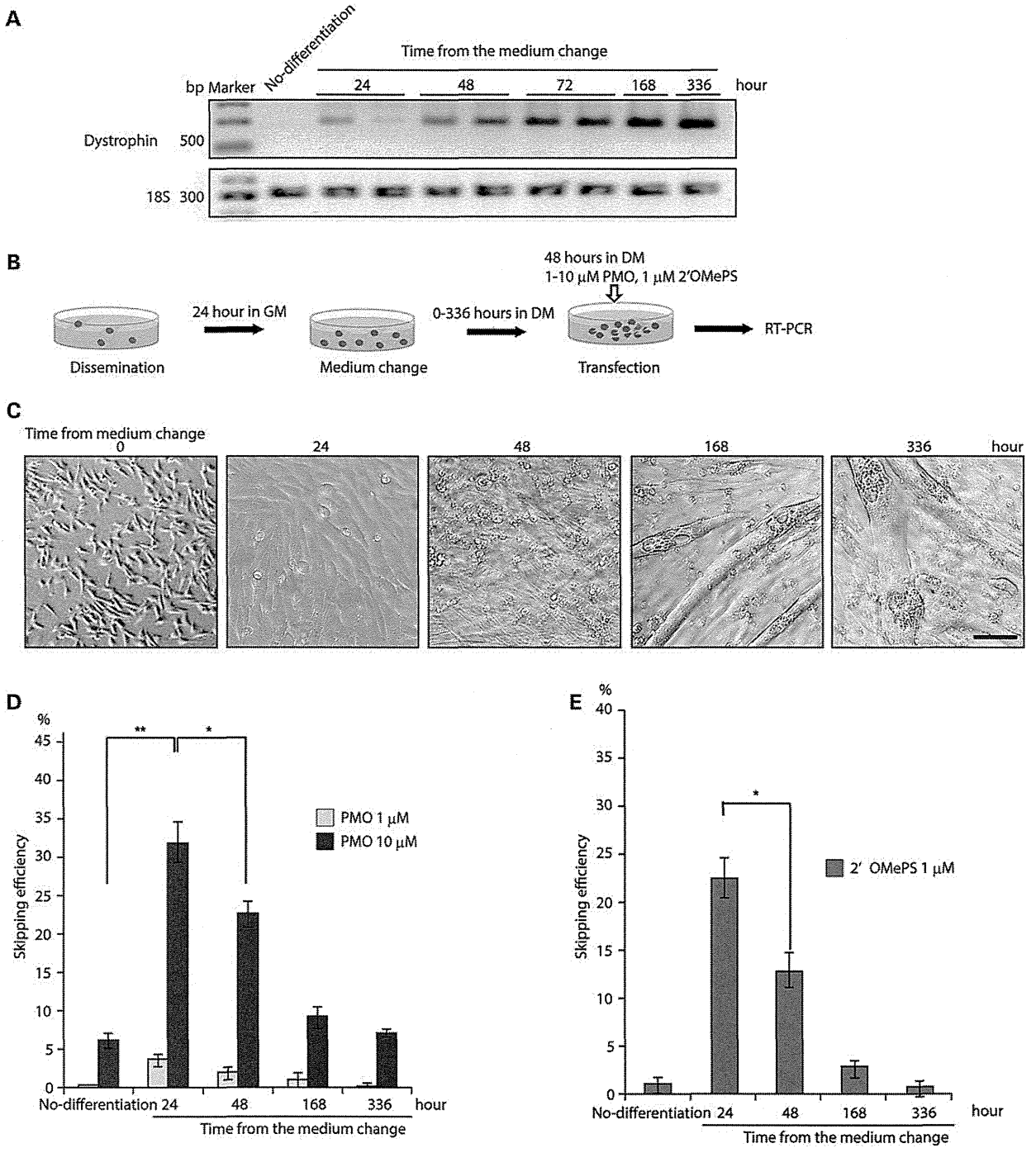

Figure 6. Evaluation of PMO or 2′OMePS uptake by C2C12 myoblasts in the differentiation process. (A) Detection of dystrophin mRNA by RT–PCR during C2C12 myoblasts differentiation. Differentiating C2C12 myoblasts were examined after a 24-, 48-, 168- or 336-h incubation and analyzed by RT–PCR. Representative data are shown. Data are representative of four independent experiments. (B) Experimental model of PMO or 2′OMePS transfection into C2C12 myoblasts. Differentiating C2C12 myoblasts were examined after a 48-h incubation with a PMO or 2′OMePS at a final concentration of 10 or 1 μM, respectively. (C) Pictures of C2C12 myoblasts at 24 h, 48 h, 7 days or 14 days after the switch from a growth medium to a differentiation medium. (D) Quantitative analysis of dystrophin expression by RT–PCR after the PMO transfection into C2C12 myoblasts is shown. The data ($n = 6$) are presented as mean ± SD. $^{**}P < 0.01$. (E) Exon 51 skipping by appropriate 2′OMePS can restore the reading frame of dystrophin in the *mdx*52 mouse. Quantitative analysis of dystrophin expression by RT–PCR after the 2′OMePS transfection into C2C12 myoblasts is shown. The data ($n = 3$) are presented as mean ± SD. $^{*}P < 0.05$.

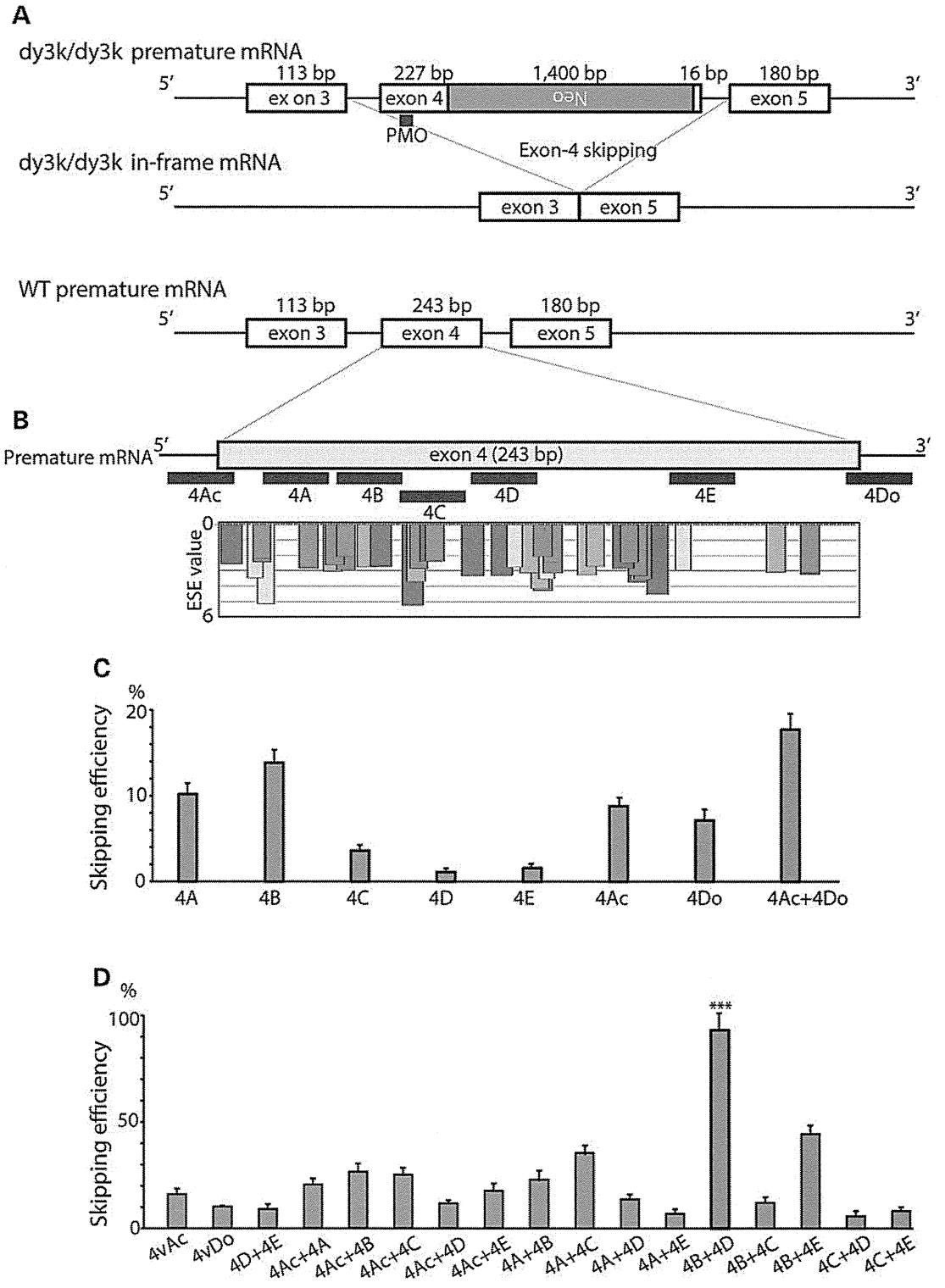

Figure 7. *In vitro* evaluation of the PMO sequences in dy^{3k}/dy^{3k} fibroblasts. (A) dy^{3k}/dy^{3k} mice have a pMC1neo polyA+ cassette (*Neo*) in exon 4 of the *Lama2* gene in the reverse direction, leading to out-of-frame products. Exon 4 skipping with PMO (black line) restores the reading frame of *Lama2* mRNA. (B) Schematic outline of the PMO targeting exon 4 of murine *Lama2* mRNA. Each PMO targets either an exonic splicing enhancer (ESE) or the 5′ or 3′ splice site, indicated by black lines. The certainties of exonic splicing enhancer sites according to ESEfinder 3.0 (46) are indicated by colored boxes. Candidates for splicing enhancer-binding proteins are shown: red, SF2/ASF; purple, SF2/ASF (IgM-BRCA1); blue, SC35; green, SRp40; yellow, SRp55. Quantitative analysis by RT–PCR of exon 4 skipping by 7 different single PMOs (C) and by 15 different combinations of two PMOs (D) in C2C12 myotubes. The data ($n = 5$) are presented as mean ± SD.

Table 3. AO sequences against exon 4 of the *Lama2* gene of mice used in this study

Name	Position	Sequence
4Ac	−19+6	GAACACCTGATGATGGGTGACAAAA
4Do	+5−20	ATGCAGCTTTTTGATCTTACCTCTC
4A	+17+41	GAATTGGCTGCCTTCACAATTACGT
4B	+45+69	TTCCAAAATCCAGTTTCCAGGCCGA
4C	+69+93	GTACTCCACGTCATCCAGGGAACGT
4D	+96+120	TGTCACCGCATGATACTGCCAGGGT
4E	+171+195	GACCTCATCATCTTTGGCGTAGGAT

Heterozygous *Lama2* gene-targeted dy^{3K} mice, which have a pMC1neo polyA+ cassette in exon 4 of the *Lama2* gene, were maintained in our animal facility. The heterozygous mice were interbred to obtain homozygous dy^{3K}/dy^{3K} mice. Genotyping of the *Lama2* deficiency was performed by PCR on tail genomic DNA. The PCR primers for the WT *Lama2* allele and the mutant allele are described in Table 4. Mice showing WT *Lama2*-negative and neo-positive PCR products were defined as *Lama2* homodeficient (dy^{3k}/dy^{3k}).

All experimental protocols in this study were approved by the Experimental Animal Care and Use Committee of the National Institute of Neuroscience, National Center of Neurology and Psychiatry, Japan.

BrdU injections

BrdU (Sigma-Aldrich, St. Louis, MO, USA) was dissolved in PBS (Gibco, Paisley, UK) and stored at 3 mg/ml at −20°C. Mice were treated with 0.8 mg/ml BrdU in their drinking water for 7 days. BrdU solution was prepared in sterile water, protected from light exposure and changed daily.

Antisense sequences and delivery methods

AO for targeted skipping of exon 51 during dystrophin pre-mRNA splicing in mice were designed to anneal to the 3′ splice site (51Do) according to our previously published report (5). The sequence was synthesized using a PMO, f-PMO (Gene Tools, LLC, Philomath, OR, USA) or 2′OMePS (Operon Biotechnologies, Tokyo, Japan). Primers for RT–PCR and sequencing analysis were synthesized by Operon Biotechnologies and are listed in Table 4.

For local studies, PMO or 2′OMePS at a dose of 400 μg/kg body weight was injected into each TA muscle of *mdx*52 mice. Muscles were obtained 2 weeks after the intramuscular injection and analyzed by RT–PCR and the cryosections by immunohistochemistry. For the systemic studies, a dose of 80–640 mg/kg PMO in 100 μl of saline or 100 μl saline was injected into the tail vein of *mdx*52 mice or WT mice, singly, and mice were examined 2 weeks after the injection. Muscles were dissected immediately, snap-frozen in liquid nitrogen-cooled isopentane and stored at −80°C for RT–PCR, immunohistochemistry and western blotting.

AO transfection

In the 2% differentiation medium, C2C12 myotubes were incubated up to 14 days. We then transfected PMO or 2′OMePS at the final concentration of 10 or 1 μM, respectively, into C2C12 myotubes without any transfection agents and incubated them for 48 h.

RT–PCR and sequencing of cDNA

Total RNA was extracted from cells or frozen tissue sections using TRIzol (Invitrogen, Carlsbad, CA, USA). Two hundred nanograms of total RNA template were used for RT–PCR with a QuantiTect Reverse Transcription Kit (Qiagen, Crawley, UK) according to the manufacturer's instructions. The cDNA product (0.5 μl) was then used as the template for PCR in a 20-μl reaction with 0.1 units of TaqDNA polymerase (Qiagen). The reaction mixture comprised 10× PCR buffer (Roche, Basel, Switzerland), 10 mM of each dNTP (Qiagen) and 10 μM of each primer. The primer sequences were Ex50F 5′-TTTACTTCGGGAGCTGAGGA-3′ and Ex53R 5′-ACCTG TTCGGCTTCTTCCTT-3′ for amplification of cDNA from exons 50 to 53. The cycling conditions were 95°C for 4 min, then 35 cycles of 94°C for 0.5 min, 60°C for 0.5 min, 72°C for 0.5 min and finally 72°C for 7 min. The intensity of PCR bands was analyzed using ImageJ software (http://rsbweb.nih.gov/ij/), and skipping efficiency was calculated by using the following formula: [(the intensity of skipped band)/(the intensity of skipped band + the intensity of unskipped band)]. After the resulting PCR bands were extracted using a gel extraction kit (Qiagen), direct sequencing of PCR products was performed by the Biomatrix Laboratory Co., Ltd. (Chiba, Japan).

Immunohistochemistry and hematoxylin and eosin staining

At least ten 8-μm cryosections were cut from flash-frozen muscles at 100-μm intervals. The serial sections were stained with polyclonal rabbit antibody P7 against the dystrophin rod domain (a gift from Dr. Qi-Long Lu, Carolinas Medical Center, Charlotte, NC, USA), monoclonal mouse antibody developmental MHC (Leica Biosystems, Newcastle Upon Tyne, UK), anti-laminin-α2 monoclonal rat antibody 4H8-2 (Abcam, Cambridge, UK) and anti-laminin polyclonal rabbit antibody L9393 (Sigma-Aldrich). Alexa-488 or 568 (Molecular Probes, Cambridge, UK) was used as a secondary antibody. DAPI containing a mounting agent (Vectashield; Vector Laboratories, Burlingame, CA, USA) was used for nuclear counterstaining. The maximum number of dystrophin-positive fibers in one section was counted, and the TA muscle fiber sizes were evaluated using a BZ-9000 fluorescence microscope (Keyence, Osaka, Japan). Hematoxylin and eosin staining was performed using Harris hematoxylin and eosin.

Western blotting

Muscle protein from cryosections was extracted with lysis buffer as described previously (5). A total of 2–20 μg protein was loaded onto a 5–15% XV Pantera Gel (DRC, Tokyo, Japan). The samples were transferred onto an Immobilon polyvinylidene fluoride membrane (Millipore, Billerica, MA, USA) by semi-dry blotting at 5 mA/mm^2 for 1.5 h. The membrane was incubated with the C-terminal monoclonal antibody Dys2 (Leica Biosystems, Newcastle Ltd.) at room temperature for 1 h. The bound primary antibody was detected by horseradish

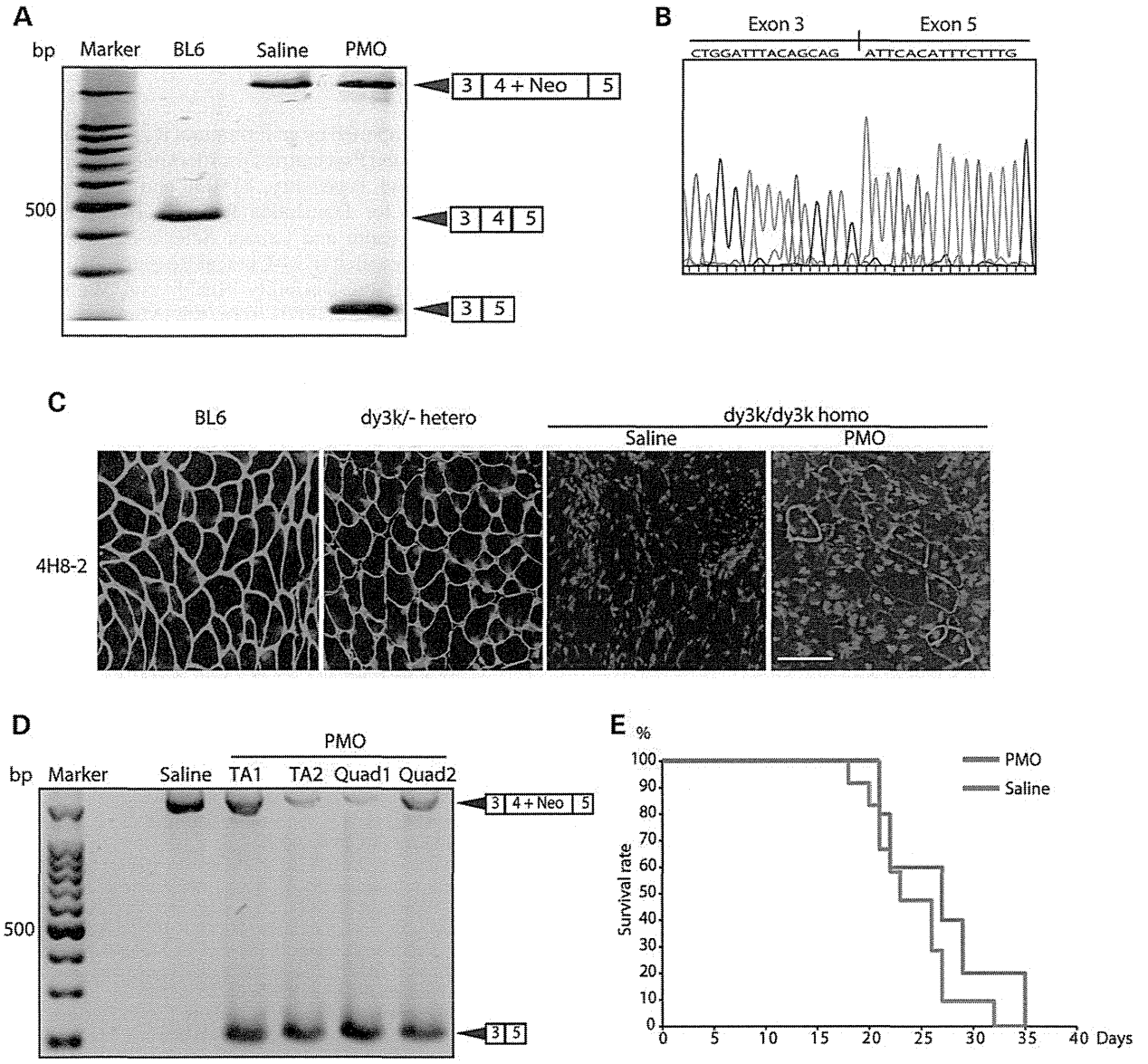

Figure 8. Recovery of laminin-α2 chain expression at the basement membrane of TA muscle in dy^{3k}/dy^{3k} mice following systemic PMO injection. (A) PMO (400 μg/kg body weight) was injected into the TA muscles of dy^{3k}/dy^{3k} mice at 5 days and RT–PCR or immunohistochemistry was performed 15 days after the injection, respectively. Effectiveness of exon 4 skipping detected by RT–PCR. Data are representative of four independent experiments. BL6: TA muscle from a WT C57/BL6. Saline: Saline-treated TA muscle from dy^{3k}/dy^{3k} mice at 10 days. PMO: Treated TA muscle from dy^{3k}/dy^{3k} mice at 25 days. $^{***}P < 0.001$. (B) Confirmation of correct exon-4 skipping by direct sequencing of the PCR products. Sequencing of the most intense band shows the exon 4-skipped *Lama2* mRNA sequence. (C) Immunohistochemical staining for laminin-α2 chain in the TA muscle. Data are representative of four independent experiments. BL6: TA muscle from a WT C57/BL6. Saline: Saline-treated TA muscle from dy^{3k}/dy^{3k} mice. PMO: PMO-treated TA muscle from dy^{3k}/dy^{3k} mice. Scale bar: 100 μm. (D and E) PMO (150 mg/kg in total) was injected intraperitoneally into the dy^{3k}/dy^{3k} mice at postnatal 4–6 days. Effectiveness of exon 4 skipping detected by RT–PCR (D). Kaplan–Meier survival analysis of saline-treated ($n = 12$) or PMO-treated dy^{3k}/dy^{3k} mice ($n = 5$) is shown (E). Quad: quadriceps. TA1 and Quad1: TA and Quad muscle from dy^{3k}/dy^{3k} mice no. 1. Quad2: TA and Quad muscle from dy^{3k}/dy^{3k} mice no. 2.

peroxidase-conjugated goat anti-mouse IgG (Cedarlane, Burlington, ON, USA) and SuperSignal chemiluminescent substrate (Pierce, Rockford, IL, USA). Anti-β-actin antibody was used as a loading control. The signal intensity of detected bands of the blots was quantified using ImageJ software and normalized to the loading control.

In situ hybridization

DNA probes with 3′-DIG tailing for *in situ* hybridization were synthesized by Nihon Gene Research Laboratories Inc. (Sendai, Japan) and are listed in Table 2. At least ten 10-μm cryosections were cut from flash-frozen muscles. The sections were

Table 4. Primer pairs for the *Dmd* or *Lama2* gene of mice used in this study

(i)	Primer pair for the *Dmd* gene
	Forward primer: 5′-TTTACTTCGGGAGCTGAGGA-3′
	Reverse primer: 5′- ACCTGTTCGGCTTCTTCCTT-3′
(ii)	Primer pair for the *Lama2* gene
	Forward primer: 5′-GGTGGCAGAGTCCCAGTATC-3′
	Reverse primer: 5′-CGATTTCTCTGGGGTCTTTG-3′
(iii)	Primer pair for the WT *Lama2* allele
	Forward primer: 5′-CCAGATTGCCTACGTAATTG-3′
	Reverse primer: 5′-CCTCTCCATTTTCTAAAG-3′
(iv)	Primer pair for the mutant *Lama2* allele
	Forward primer: 5′-CTTGGGTGGAGAGGCTATTC-3′
	Reverse primer: 5′-AGGTGAGATGACAGGAGATC-3′

fixed in 4% paraformaldehyde for 30 min and dehydrated for 16 h at 42°C. The sections were incubated in HCl (0.2 N) for 20 min and subjected to pretreatment with proteinase K (1 μg/ml) for 15 min at 37°C. The sections were fixed in 4% paraformaldehyde for 5 min at room temperature and then incubated in glycine (10 mg/ml) for 15 min. Next, sections were subjected to incubation for 2 h in prehybridization solution: 40% deionized formamide and 4 × SSC buffer. The sections were hybridized for 14 h at 30°C in a hybridization solution containing 3 μg/ml of digoxigenin-labeled probe. The sections were then washed sequentially for 60 min with 2× SSC, 1× SSC and 0.5× SSC. The final wash was with 0.1× SSC for 40 min. For detection of digoxigenin-labeled probe, anti-digoxigenin–alkaline phosphatase (Roche) and NBT/BCIP Stock Solution (Roche) were used according to the manufacturer instructions. After the development, slides were counterstained with hematoxylin/eosin. The *in situ* hybridization solution contained 40% formamide (Sigma-Aldrich), 10 mM Tris (pH 7.5), 1× Denhardt's solution, 1 mM EDTA, 20% dextran sulfate (Pharmacia, Basking Ridge, NJ, USA), 5 M NaCl, 0.25 mg of salmon DNA and 0.25 mg of yeast tRNA.

Statistical analysis

Statistical differences were assessed by one-way analysis of variance with differences among the groups assessed by a Tukey's comparison or Fisher's exact test. All data are reported as mean values ± SD or SEM. The level of significance was set at $P < 0.05$.

SUPPLEMENTARY MATERIAL

Supplementary Material is available at *HMG* online.

ACKNOWLEDGEMENTS

The authors thank Yuko Suzuki and Michihiro Imamura for insightful discussions about this study. We thank Takashi Saito, Jun Tanihata, Yuko-Motohashi Shimizu, Satoru Masuda, Hayashiji Nozomi and Ryoko Nakagawa for useful discussions and technical assistance. We also thank Kenji Kuwabara, Kazushi Takagaki, Satoru Sonoke, Kaoru Fujiwara and other members of Nippon Shinyaku Co Ltd.

Conflict of Interest statement. None declared.

FUNDING

This work was supported by an Intramural Research Grant (22-5) for Neurological and Psychiatric Disorders of the National Center of Neurology and Psychiatry, Health and Labour Sciences Research Grants for Translation Research (H21-Translational Research-011), Health and Labour Sciences Research Grants for Translation Research (H21-Clinical Research-015), Comprehensive Research on Disability Health and Welfare (H23-Neuromuscular Disease-005) from the Ministry of Health, Labour, and Welfare of Japan and MRC Confidence in Concept Award (CiC17).

REFERENCES

1. Hoffman, E.P., Brown, R.H. and Kunkel, L.M. (1987) Dystrophin: the protein product of the Duchenne muscular dystrophy locus. *Cell*, **51**, 919–928.
2. Monaco, A.P., Bertelson, C.J., Liechti-Gallati, S., Moser, H. and Kunkel, L.M. (1988) An explanation for the phenotypic differences between patients bearing partial deletions of the DMD locus. *Genomics*, **2**, 90–95.
3. Matsuo, M., Masumura, T., Nishio, H., Nakajima, T., Kitoh, Y., Takumi, T., Koga, J. and Nakamura, H. (1991) Exon skipping during splicing of dystrophin mRNA precursor due to an intraexon deletion in the dystrophin gene of Duchenne muscular dystrophy Kobe. *J. Clin. Invest.*, **87**, 2127–2131.
4. Wood, M.J.A. (2010) Toward an oligonucleotide therapy for Duchenne muscular dystrophy: a complex development challenge. *Sci. Transl. Med.*, **2**, 25ps15.
5. Aoki, Y., Nakamura, A., Yokota, T., Saito, T., Okazawa, H., Nagata, T. and Takeda, S. (2010) In-frame dystrophin following exon 51-skipping improves muscle pathology and function in the exon 52-deficient mdx mouse. *Mol. Ther.*, **18**, 1995–2005.
6. Aoki, Y., Yokota, T., Nagata, T., Nakamura, A., Tanihata, J., Saito, T., Duguez, S.M.R., Nagaraju, K., Hoffman, E.P., Partridge, T. *et al.* (2012) Bodywide s kipping of exons 45–55 in dystrophic mdx52 mice by systemic antisense delivery. *Proc. Natl. Acad. Sci. USA*, **109**, 13763–13768.
7. Yokota, T., Lu, Q.-L., Partridge, T., Kobayashi, M., Nakamura, A., Takeda, S. and Hoffman, E. (2009) Efficacy of systemic morpholino exon-skipping in Duchenne dystrophy dogs. *Ann. Neurol.*, **65**, 667–676.
8. Lu, Q.L., Rabinowitz, A., Chen, Y.C., Yokota, T., Yin, H., Alter, J., Jadoon, A., Bou-Gharios, G. and Partridge, T. (2005) Systemic delivery of antisense oligoribonucleotide restores dystrophin expression in body-wide skeletal muscles. *Proc. Natl. Acad. Sci. USA*, **102**, 198–203.
9. Cirak, S., Arechavala-Gomeza, V., Guglieri, M., Feng, L., Torelli, S., Anthony, K., Abbs, S., Garralda, M.E., Bourke, J., Wells, D.J. *et al.* (2011) Exon skipping and dystrophin restoration in patients with Duchenne muscular dystrophy after systemic phosphorodiamidate morpholino oligomer treatment: an open-label, phase 2, dose-escalation study. *Lancet*, **378**, 595–605.
10. Goemans, N.M., Tulinius, M., Van den Akker, J.T., Burm, B.E., Ekhart, P.F., Heuvelmans, N., Holling, T., Janson, A.A., Platenburg, G.J., Sipkens, J.A. *et al.* (2011) Systemic administration of PRO051 in Duchenne's muscular dystrophy. *N. Engl. J. Med.*, **364**, 1513–1522.
11. Arora, V., Devi, GR. and Iversen, PL. (2004) Neutrally charged phosphorodiamidate morpholino antisense oligomers: uptake, efficacy and pharmacokinetics. *Curr. Pharm. Biotechnol.*, **5**, 431–439.
12. Ghosh, C. and Iversen, P.L. (2000) Intracellular delivery strategies for antisense phosphorodiamidate morpholino oligomers. *Antisense Nucleic Acid Drug Dev.*, **10**, 263–274.
13. Petrof, B.J., Shrager, J.B., Stedman, H.H., Kelly, A.M. and Sweeney, H.L. (1993) Dystrophin protects the sarcolemma from stresses developed during muscle contraction. *Proc. Natl. Acad. Sci. USA*, **90**, 3710–3714.
14. McArdle, A., Edwards, R.H. and Jackson, M.J. (1994) Time course of changes in plasma membrane permeability in the dystrophin-deficient mdx mouse. *Muscle Nerve*, **17**, 1378–1384.

15. Araki, E., Nakamura, K., Nakao, K., Kameya, S., Kobayashi, O., Nonaka, I., Kobayashi, T. and Katsuki, M. (1997) Targeted disruption of exon 52 in the mouse dystrophin gene induced muscle degeneration similar to that observed in Duchenne muscular dystrophy. *Biochem. Biophys. Res. Commun.*, **238**, 492–497.
16. Miyagoe, Y., Hanaoka, K., Nonaka, I., Hayasaka, M., Nabeshima, Y., Arahata, K. and Takeda, S. (1997) Laminin alpha2 chain-null mutant mice by targeted disruption of the Lama2 gene: a new model of merosin (laminin 2)-deficient congenital muscular dystrophy. *FEBS Lett.*, **415**, 33–39.
17. Saito, T., Nakamura, A., Aoki, Y., Yokota, T., Okada, T., Osawa, M. and Takeda, S. (2010) Antisense PMO found in dystrophic dog model was effective in cells from Exon 7-deleted DMD patient. *PLoS ONE*, **5**, 8.
18. Amantana, A. and Iversen, PL. (2005) Pharmacokinetics and biodistribution of phosphorodiamidate morpholino antisense oligomers. *Curr. Opin. Pharmacol.*, **5**, 550–555.
19. Hudziak, R.M., Barofsky, E., Barofsky, D.F., Weller, D.L., Huang, S.B. and Weller, D.D. (1996) Resistance of morpholino phosphorodiamidate oligomers to enzymatic degradation. *Antisense Nucleic Acid Drug Dev.*, **6**, 267–272.
20. Moulton, H.M. and Moulton, J.D. (2010) Morpholinos and their peptide conjugates: therapeutic promise and challenge for Duchenne muscular dystrophy. *Biochim. Biophys. Acta*, **1798**, 2296–2303.
21. Popplewell, L.J., Malerba, A. and Dickson, G. (2012) Optimizing antisense oligonucleotides using phosphorodiamidate morpholino oligomers. *Methods Mol. Biol.*, **867**, 143–167.
22. Iversen, P.L., Aird, K.M., Wu, R., Morse, M.M. and Devi, G.R. (2009) Cellular uptake of neutral phosphorodiamidate morpholino oligomers. *Curr. Pharm. Biotechnol.*, **10**, 579–588.
23. Mokri, B. and Engel, A.G. (1975) Duchenne dystrophy: electron microscopic findings pointing to a basic or early abnormality in the plasma membrane of the muscle fiber. *Neurology*, **25**, 1111–1120.
24. Yokota, T., Takeda, S., Lu, Q.-L., Partridge, T.A., Nakamura, A. and Hoffman, E.P. (2009) A renaissance for antisense oligonucleotide drugs in neurology: exon skipping breaks new ground. *Arch. Neurol.*, **66**, 32–38.
25. Hoffman, E.P., Bronson, A., Levin, A.A., Takeda, S., Yokota, T., Baudy, A.R. and Connor, E.M. (2011) Restoring dystrophin expression in Duchenne muscular dystrophy muscle progress in exon skipping and stop codon read through. *Am. J. Pathol.*, **179**, 12–22.
26. Florence, J.M., Fox, P.T., Planer, G.J. and Brooke, M.H. (1985) Activity, creatine kinase, and myoglobin in Duchenne muscular dystrophy: a clue to etiology? *Neurology*, **35**, 758–761.
27. Ozawa, E. (2010) Our trails and trials in the subsarcolemmal cytoskeleton network and muscular dystrophy researches in the dystrophin era. *Proc. Jpn. Acad. Ser. B Phys. Biol. Sci.*, **86**, 798–821.
28. Heemskerk, H., De Winter, C., Van Kuik, P., Heuvelmans, N., Sabatelli, P., Rimessi, P., Braghetta, P., Van Ommen, G.-J.B., De Kimpe, S., Ferlini, A. *et al.* (2010) Preclinical PK and PD studies on 2′-O-methyl-phosphorothioate RNA antisense oligonucleotides in the mdx mouse model. *Mol. Ther.*, **18**, 1210–1217.
29. Matsuda, R., Nishikawa, A. and Tanaka, H. (1995) Visualization of dystrophic muscle fibers in mdx mouse by vital staining with Evans blue: evidence of apoptosis in dystrophin-deficient muscle. *J. Biochem.*, **118**, 959–964.
30. Straub, V., Rafael, J.A., Chamberlain, J.S. and Campbell, K.P. (1997) Animal models for muscular dystrophy show different patterns of sarcolemmal disruption. *J. Cell Biol.*, **139**, 375–385.
31. Wood, M.J.A., Gait, M.J. and Yin, H. (2010) RNA-targeted splice-correction therapy for neuromuscular disease. *Brain*, **133**, 957–972.
32. Nakamura, A. and Takeda, S. (2011) Exon-skipping therapy for Duchenne muscular dystrophy. *Lancet*, **378**, 546–547.
33. Yokota, T., Nakamura, A., Nagata, T., Saito, T., Kobayashi, M., Aoki, Y., Echigoya, Y., Partridge, T., Hoffman, E.P. and Takeda, S. (2012) Extensive and prolonged restoration of dystrophin expression with vivo-morpholino-mediated multiple exon skipping in dystrophic dogs. *Nucleic Acid Ther.*, **22**, 306–315.
34. Ezzat, K., Helmfors, H., Tudoran, O., Juks, C., Lindberg, S., Padari, K., El-Andaloussi, S., Pooga, M. and Langel, U. (2012) Scavenger receptor-mediated uptake of cell-penetrating peptide nanocomplexes with oligonucleotides. *FASEB J.*, **26**, 1172–1180.
35. Moulton, H.M., Fletcher, S., Neuman, B.W., McClorey, G., Stein, D.A., Abes, S., Wilton, S.D., Buchmeier, M.J., Lebleu, B. and Iversen, P.L. (2007) Cell-penetrating peptide-morpholino conjugates alter pre-mRNA splicing of DMD (Duchenne muscular dystrophy) and inhibit murine coronavirus replication in vivo. *Biochem. Soc. Trans.*, **35**, 826–828.
36. Yin, H., Moulton, H.M., Betts, C., Merritt, T., Seow, Y., Ashraf, S., Wang, Q., Boutilier, J. and Wood, M.J. (2010) Functional rescue of dystrophin-deficient mdx mice by a chimeric peptide-PMO. *Mol. Ther.*, **18**, 1822–1829.
37. Moulton, H.M., Nelson, M.H., Hatlevig, S.A., Reddy, M.T. and Iversen, P.L. (2004) Cellular uptake of antisense morpholino oligomers conjugated to arginine-rich peptides. *Bioconjug. Chem.*, **15**, 290–299.
38. Amantana, A., Moulton, H.M., Cate, M.L., Reddy, M.T., Whitehead, T., Hassinger, J.N., Youngblood, D.S. and Iversen, P.L. (2007) Pharmacokinetics, biodistribution, stability and toxicity of a cell-penetrating peptide-morpholino oligomer conjugate. *Bioconjug. Chem.*, **18**, 1325–1331.
39. Henry, S.P., Giclas, P.C., Leeds, J., Pangburn, M., Auletta, C., Levin, A.A. and Kornbrust, D.J. (1997) Activation of the alternative pathway of complement by a phosphorothioate oligonucleotide: potential mechanism of action. *J. Pharmacol. Exp. Ther.*, **281**, 810–816.
40. Sheehan, J.P. and Lan, H.C. (1998) Phosphorothioate oligonucleotides inhibit the intrinsic tenase complex. *Blood*, **92**, 1617–1625.
41. Hawke, T.J. and Garry, D.J. (2001) Myogenic satellite cells: physiology to molecular biology. *J. Appl. Physiol.*, **91**, 534–551.
42. Miyagoe-Suzuki, Y., Nakagawa, M. and Takeda, S. (2000) Merosin and congenital muscular dystrophy. *Microsc. Res. Tech.*, **48**, 181–191.
43. Gawlik, K.I. and Durbeej, M. (2011) Skeletal muscle laminin and MDC1A: pathogenesis and treatment strategies. *Skeletal Muscle*, **1**, 9.
44. Sunada, Y., Bernier, S.M., Utani, A., Yamada, Y. and Campbell, K.P. (1995) Identification of a novel mutant transcript of laminin alpha 2 chain gene responsible for muscular dystrophy and dysmyelination in dy2J mice. *Hum. Mol. Genet.*, **4**, 1055–1061.
45. Allamand, V. and Guicheney, P. (2002) Merosin-deficient congenital muscular dystrophy, autosomal recessive (MDC1A, MIM#156225, LAMA2 gene coding for alpha2 chain of laminin). *Eur. J. Hum. Genet.*, **10**, 91–94.
46. Cartegni, L., Wang, J., Zhu, Z., Zhang, MQ. and Krainer, AR. (2003) ESEfinder: A web resource to identify exonic splicing enhancers. *Nucleic Acids Res.*, **31**, 3568–3571.

Identification of Disease Specific Pathways Using *in Vivo* SILAC Proteomics in Dystrophin Deficient *mdx* Mouse*[S]

Sree Rayavarapu‡§, William Coley‡§, Erdinc Cakir‡, Vanessa Jahnke‡, Shin'ichi Takeda¶, Yoshitsugu Aoki¶, Heather Grodish-Dressman‡, Jyoti K. Jaiswal‡§, Eric P. Hoffman‡§, Kristy J. Brown‡§, Yetrib Hathout‡§, and Kanneboyina Nagaraju‡§‖

Duchenne muscular dystrophy (DMD) is an X-linked neuromuscular disorder caused by a mutation in the dystrophin gene. DMD is characterized by progressive weakness of skeletal, cardiac, and respiratory muscles. The molecular mechanisms underlying dystrophy-associated muscle weakness and damage are not well understood. Quantitative proteomics techniques could help to identify disease-specific pathways. Recent advances in the *in vivo* labeling strategies such as stable isotope labeling in mouse (SILAC mouse) with $^{13}C_6$-lysine or stable isotope labeling in mammals (SILAM) with ^{15}N have enabled accurate quantitative analysis of the proteomes of whole organs and tissues as a function of disease. Here we describe the use of the SILAC mouse strategy to define the underlying pathological mechanisms in dystrophin-deficient skeletal muscle. Differential SILAC proteome profiling was performed on the gastrocnemius muscles of 3-week-old (early stage) dystrophin-deficient mdx mice and wild-type (normal) mice. The generated data were further confirmed in an independent set of mdx and normal mice using a SILAC spike-in strategy. A total of 789 proteins were quantified; of these, 73 were found to be significantly altered between mdx and normal mice ($p < 0.05$). Bioinformatics analyses using Ingenuity Pathway software established that the integrin-linked kinase pathway, actin cytoskeleton signaling, mitochondrial energy metabolism, and calcium homeostasis are the pathways initially affected in dystrophin-deficient muscle at early stages of pathogenesis. The key proteins involved in these pathways were validated by means of immunoblotting and immunohistochemistry in independent sets of mdx mice and in human DMD muscle biopsies. The specific involvement of these molecular networks early in dystrophic pathology makes them potential therapeutic targets. In sum, our findings indicate that SILAC mouse strategy has uncovered previously unidentified pathological pathways in mouse models of human skeletal muscle disease. ***Molecular & Cellular Proteomics 12: 10.1074/mcp.M112.023127, 1061–1073, 2013.***

Dystrophin is an essential skeletal muscle protein that interacts with other glycoproteins such as the dystroglycans and sarcoglycans to form the dystrophin glycoprotein complex. This complex links the extracellular matrix and the cytoskeleton of the myofiber via F-actin, thereby protecting the skeletal muscle membrane against contraction-induced damage (1). The absence of this complex due to the lack of expression of dystrophin makes the myofiber membrane susceptible to damage, which in turn activates various pathogenic processes and aberrant signaling cascades (2–4). Immune-mediated mechanisms are considered one of the key contributors to muscle degeneration in dystrophin-deficient subjects. However, the explicit role of specific pathogenic processes in this disease has not been thoroughly investigated.

Dystrophin-deficient mdx mice are one of the most widely used animal models for studying disease pathophysiology and testing various therapeutic regimens (5). The mdx-23 mouse model on a C57BL/10 background is a spontaneous mutant with a point mutation in exon 23 of the dystrophin gene that eliminates the expression of dystrophin (6). However, this mutation does not disrupt the expression of shorter isoforms that are also expressed from the dystrophin gene through differential promoter usage. Another mutant mdx mouse model, mdx-52 on a C57BL/6 background, has been generated by disrupting the dystrophin gene through gene targeting and the deletion of exon 52. The mdx-52 mice lack both dystrophin and the shorter dystrophin isoforms (Dp140 and Dp260). The skeletal muscles of mdx-52 mice exhibit a pathological profile similar to that of mdx-23 mice (7). These mdx strains show a mild phenotype relative to the human disease, but nevertheless display substantial myofiber degeneration, muscle weakness, elevated serum creatine kinase,

From the ‡Research Center for Genetic Medicine, Children's National Medical Center, 111 Michigan Ave NW, Washington, D.C.; §Institute of Biomedical Sciences, Department of Integrative Systems Biology, The George Washington University, 2300 Eye Street NW, Ross 605, Washington, D.C.; ¶Department of Molecular Therapy, National Institute of Neuroscience, National Center of Neurology and Psychiatry, 4-1-1 Ogawa-higashi, Kodaira, Tokyo

Received August 21, 2012, and in revised form, November 8, 2012
Published, MCP Papers in Press, January 7, 2013, DOI 10.1074/mcp.M112.023127

and extensive inflammatory infiltrates in the muscle tissue (5, 8). Initial disease onset in mdx mice occurs around 3 weeks of age, with recurring bouts of myofiber degeneration and regeneration. These bouts are limited by 12 to 16 weeks of age, but the tissue infiltration and muscle weakness continue for the remainder of the animal's life. Thus, this model continues to be important for studying the consequences of dystrophin deficiency and alteration in the molecular events that lead to muscle pathology. For our studies, we have used mdx-52 mice that are on the C57BL/6 background.

The investigation of protein dynamics and their involvement in signaling pathways in the course of dystrophinopathy can provide valuable insight into its pathogenesis. Protein modulations can be monitored using mass-spectrometry-based quantitative strategies. In the past, two-dimensional gel electrophoresis and fluorescence difference in gel electrophoresis methods have been used to study protein changes in the muscle of dystrophic mdx mice. Traditional proteomic techniques (2-DE) suffer from a disadvantage in that they detect alterations predominantly in abundantly expressed proteins. Furthermore, prior studies using the mdx mouse model focused on established disease instead of early disease, in which limited pathways drive the pathology. Proteomic profiling of established disease has identified perturbations in Ca^{2+} handling and bioenergetic pathways but not specific mechanisms that are upstream in the pathogenesis (9–12). Therefore, we performed proteomic studies of early disease stages in the mdx mouse model.

The stable isotope labeling by amino acids in cell culture (SILAC)[1] strategy introduced by Ong *et al.* has been successfully implemented in various cell culture systems and has been proven to be the most accurate method for proteome profiling (13–17). More recently, this powerful technique has been extended to *in vivo* studies to develop heavy-stable-isotope-labeled mammals. This method has been evaluated in both mice (SILAC mouse) and rats (SILAM) (18–20). In the SILAC mouse strategy, the mice feed consists of a balanced synthetic feed labeled with $^{13}C_6$-Lys, whereas in SILAM, the feed consists of ^{15}N-labeled algae. These techniques enabled accurate measurement of differentially expressed proteins in different organs and tissues of mice and rats under different conditions (18, 19, 21–23). Here we have extended the use of the SILAC mouse strategy to study the underlying molecular alterations in gastrocnemius muscle in the early phase of dystrophic muscle disease. To our knowledge, this is the first proteomics study of dystrophic skeletal muscle using an *in vivo* labeling strategy. With this method, we have not only confirmed the previously identified pathways (mitochondria and energy metabolism) that are differentially modulated in Duchenne muscular dystrophy (DMD), but also uncovered novel pathways such as actin cytoskeletal and integrin-linked kinase (ILK) signaling pathways that are implicated in dystrophic pathology.

[1] The abbreviations used are: DMD, Duchenne muscular dystrophy; ILK, integrin-linked kinase; IPA, Ingenuity Pathway Analysis; SILAC, stable isotope labeling with amino acids in cell culture.

MATERIALS AND METHODS

Animals and Feed—C57BL/6 control mice and dystrophin-deficient mdx-52 mice weighing 20 to 25 g were used for breeding to generate SILAC-labeled and unlabeled mice using custom-made mouse feed as described below. The mdx-52 mice were on a C57BL/6 background (7). All animals were handled according to Institutional Animal Care and Use Committee guidelines at the Children's National Medical Center (Approved Protocol No. 199-07-01).

Generating ^{13}C-lysine-C57BL/6-SILAC Mice—We followed the method described by Kruger *et al.* to generate SILAC mice (18). Mouse-Express feed containing "heavy" L-lysine ($^{13}C_6$, 99%) or "light" L-lysine ($^{12}C_6$, 99%) at the 1% level that adhered to standard laboratory mouse nutritional standards was purchased from Cambridge Isotope Laboratories (Andover, MA). In this study, we arbitrarily chose to label wild-type C57BL/6 mice. Breeding pairs were set up, and after the confirmation of pregnancy, dams were fed the custom $^{13}C_6$-lysine diet and breeding was continued to obtain F2-generation litters. In parallel, dystrophin-deficient mdx-52 breeding pairs were maintained on unlabeled custom feed ($^{12}C_6$-lysine) and bred to obtain F2-generation mdx litters.

For all validation experiments, an independent set of C57BL/6 and mdx-52 mice (n = 3/group) that had been maintained on non-custom (normal) feed was used. All animals were housed in an individually vented cage system under a controlled 12-hour light/dark cycle with free access to feed and water.

Sample Collection—SILAC mice and age-matched mdx mice were perfused with phosphate-buffered saline to remove excess blood from organs and tissues and were then euthanized using CO_2. All organs including muscle tissues were harvested and flash-frozen in liquid nitrogen-chilled isopentane. The collected tissues were stored at −80 °C until use. Liver, gastrocnemius, and brain were collected from "labeled" C57BL/6 mice of each generation (F0, F1, and F2) in order to monitor the incorporation of ^{13}C-lysine. For differential proteomic analysis between normal and dystrophic mdx mice, tissues were collected from F2-generation labeled C57BL/6 mice and age-matched unlabeled mdx mice. Tissues were collected at 3, 6, and 12 weeks of age from labeled C57BL/6 and mdx mice (n = 2/age group) for this study, as well as for other projects. In the current study, we analyzed 3-week-old mdx gastrocnemius to identify early changes in the dystrophic skeletal muscle proteome.

Monitoring Labeling Efficiency ($^{13}C_6$-lysine) in SILAC Mouse Tissues—Protein lysates were prepared from tissue samples harvested from the labeled C57BL/6 at F0, F1, and F2 generations. Aliquots (50 μg) of protein lysate from each extract were separated via SDS-PAGE and stained with Bio-Safe Coomassie (Bio-Rad, Hercules, CA). Individual bands were excised and digested with trypsin, and the resulting peptides were analyzed via LC-MS/MS as described below. Raw spectra were analyzed using Integrated Proteomics Pipeline (IP2) software (version 1.01), developed by Integrated Proteomics Applications, Inc (San Diego, CA). Labeling efficiency was determined from unlabeled to labeled peptide ratios obtained for all identified proteins in each tissue (liver, brain, and muscle). These ratios were converted into percentages and then averaged to obtain the overall labeling efficiency for each respective tissue at each generation.

Sample Processing and Mass Spectrometry Analysis to Identify Proteomic Alterations—Gastrocnemius muscle was collected from 3-week-old F2-generation SILAC-labeled C57BL/6 mice and age-matched unlabeled dystrophic mdx mice. Gastrocnemius muscle was also collected from age-matched unlabeled C57BL/6 mice. Total proteins were extracted from each muscle with RIPA buffer (50 mM

Tris-HCl, pH 8.0, with 150 mM sodium chloride, 1.0% Igepal CA-630 (Nonidet P-40), 0.5% sodium deoxycholate, and 0.1% sodium dodecyl sulfate) with protease inhibitors (Halt protease inhibitor mixture 100X). Aliquots of the protein extracts from the muscles of unlabeled C57BL/6 and unlabeled mdx mice were each mixed 1:1 (50 μg) with protein extract from the muscle of a SILAC-labeled mouse. The protein concentration was estimated via BCA protein assay (Pierce). Labeled and unlabeled protein mixtures were further resolved via SDS-PAGE. The gel was stained with Bio-Safe Coomassie (Bio-Rad, Hercules, CA), and each lane was cut into 30 to 35 serial slices. Proteins in each gel slice were in-gel digested with trypsin. The resulting peptides from each band were injected via an autosampler (6 μl) and loaded onto a Symmetry C18 trap column (5 μm, 300 μm inner diameter × 23 mm, Waters Milford, MA) for 10 min at a flow rate of 10 μl/min with 0.1% formic acid. The sample was subsequently separated on a C18 reversed-phase column (3.5 μm, 75 μm × 15 cm, LC Packings Sunnyvale, CA) at a flow rate of 250 nl/min using a Nano-HPLC system from Eksigent (Dublin, CA). The mobile phases consisted of water with 0.1% formic acid (A) and 90% acetonitrile (B). A 65-min linear gradient from 5% to 40% B was employed. Eluted peptides were introduced into the mass spectrometer via a 10-μm silica tip (New Objective Inc., Ringoes, NJ) adapted to a nano-electrospray source (ThermoFisher Scientific). The spray voltage was set at 1.2 kV, and the heated capillary at 200 °C. The LTQ-Orbitrap-XL (ThermoFisher Scientific) was operated in data-dependent mode with dynamic exclusion, in which one cycle of experiments consisted of a full MS survey scan in the Orbitrap (300–2000 *m/z*, resolution = 30,000) and five subsequent MS/MS scans in the LTQ of the most intense peaks, using collision-induced dissociation with the collision gas (helium) and normalized collision energy value set at 35%.

Database Search and SILAC Ratio Measurement—Protein identification and quantification were performed using IP2 software (version 1.01). Mass spectral data were uploaded into the IP2 software. Files from each lane were searched against the forward and reverse Uniprot mouse database (UniProt release 15.15, March 2010, 16,333 forward entries) for partially tryptic peptides, allowing two missed cleavages and the possible modification of oxidized methionine (15.99492 Da) and heavy Lys (6.020 Da). IP2 uses the Sequest 2010 (06 10 13 1836) search engine. The mass tolerance was set at ±30 ppm for MS and ±1.5 Da for MS/MS. Data were filtered by setting the protein false discovery rate at less than 1%. Only proteins that were identified by at least two unique peptides were retained for further quantitative analysis. Census software (version 1.77), built into the IP2 platform, was used to determine the ratios of unlabeled to labeled peptide using an extracted chromatogram approach. Quantitative data were filtered based on a determinant value of 0.5 and an outlier *p* value of 0.1.

Data Validation Using Spike-in Strategy—To increase the robustness and to statistically validate the data obtained in the initial differential SILAC experiments using mdx and wild-type mice, we employed a spike-in SILAC strategy that was previously used in cell culture systems (24, 25). In brief, gastrocnemius muscle lysates were obtained from both unlabeled C57BL/6 ($n = 3$) and unlabeled mdx ($n = 3$) mice. These lysates were spiked with equal amounts of lysate from labeled C57BL6 mice that was used as reference. Downstream sample preparation and MS analysis were performed as described above. To identify significant protein alterations between the mdx and wild-type groups, the mean relative ratio (unlabeled/labeled values) was compared for each protein between mdx ($n = 3$) and control ($n = 3$) mice using a non-parametric Wilcoxon rank sum test. Significance was set at $p < 0.05$, and no adjustments for multiple testing were performed.

Ingenuity Pathway Analysis to Determine the Molecular Mechanisms Implicated in Dystrophic Muscle—A bioinformatics approach was used to elucidate the global implications of differentially expressed proteins in dystrophic muscle. Ingenuity computational pathway analysis (IPA) (Ingenuity Systems, Redwood City, CA) software was applied to identify potentially perturbed molecular pathways in dystrophic muscle. The IPA program uses a knowledge database derived from the literature to relate the proteins to each other based on their interaction and function. The knowledge base consists of a high-quality expert-curated database containing 1.5 million biological findings consisting of more than 42,000 mammalian genes and pathway interactions extracted from the literature. In brief, proteins that were confidently identified in at least two samples (of both C57BL/6 and mdx comparisons) were considered for IPA analysis. All proteins that fell into the specified criteria were shortlisted, SILAC ratios were converted to fold changes and uploaded into the IPA software. Ingenuity then used these proteins and their identifiers to navigate the curated literature database and extract the overlapping network(s) among the candidate proteins. Associated networks were generated, along with a score representing the log probability of a particular network being found by random chance. Top canonical pathways associated with the uploaded data were presented, along with a *p* value. The *p* values were calculated using right-tailed Fisher's exact tests.

Validation Using Biochemical Assays—

Immunoblotting—Gastrocnemius protein lysates (25 μg of protein) from dystrophic ($n = 3$) and control ($n = 3$) muscles were mixed with 4x NuPage LDS buffer (Invitrogen) supplemented with 50 mM DTT, heated for 5 min at 85 °C, loaded on Novex® 4%–12% Tris acetate mini gels (Invitrogen), and electrophoresed at 150 V in MOPS running buffer (20X) for 90 min at room temperature. Separated proteins were transferred at 300 mA for 90 min at room temperature onto a nitrocellulose membrane (Millipore Billerica, MA). Membranes were blocked in TBS-T (20 mM Tris, 500 mM NaCl, pH 7.5, with 0.1% Tween 20) supplemented with 5% nonfat dry milk (Bio-Rad) for 1 h at room temperature. The membranes were then incubated overnight at 4 °C with primary antibodies against desmin (1:2000; Santa Cruz), annexin-2 (1:1000; Santa Cruz), ILK (1:1000; Santa Cruz), vimentin, cofilin, and profilin (1:1000; Epitomics Burlingame, CA). All antibodies were diluted in TBS-T-5% milk. Membranes were washed three times (for 10 min each time) in TBS-T and incubated with goat anti-rabbit or rabbit anti-mouse secondary antibodies (Dako, Carpinteria, CA) conjugated to horseradish peroxidase (1:3000 in TBS-T-5% milk) for 1 h at room temperature. The protein bands were revealed with ECL chemi-luminescence substrate (Amersham Biosciences). Membranes were then stripped and exposed to β-actin antibody as a loading control. For quantification, the x-ray films were scanned, and densitometry analysis was carried out using a BioRad GS-800 calibrated densitometer running Quantity One software (Bio-Rad). Ratios of the optical density of each specific protein to the corresponding β-actin were compared between mdx and C57BL/6 samples in order determine significant differences.

Lactate Dehydrogenase and Citrate Synthase activity—Lactate dehydrogenase activity was monitored in mdx ($n = 3$) and C57BL/6 ($n = 3$) muscle lysates as described earlier (26). In brief, 2.5 μl of protein extract (1:2 dilution) and 225 μl of assay buffer (2.5 ml of 1 M Tris (pH 7.6), 500 μl of 200 mM EDTA, 500 μl of 5 mM $NADH,H^+$, and 48 ml water) were used to measure enzyme activity. The oxidation of $NADH,H^+$ was recorded after pyruvate addition (10 μl, 100 mM). NADH fluorescence was detected using a luminescence/fluorescence analyzer (Mithras LB 940, Berthold Technologies Bad Wildbad, Germany). Lactate dehydrogenase activity was normalized to the protein concentration and expressed as the mean ± S.E.

Citrate synthase activity (EC 4.1.3.7) was measured in mdx ($n = 3$) and C57BL/6 ($n = 3$) muscle lysates as described earlier (26). In brief, 2.5 μl of protein extract (1:30 dilution, v/v) was added to 225 μl of

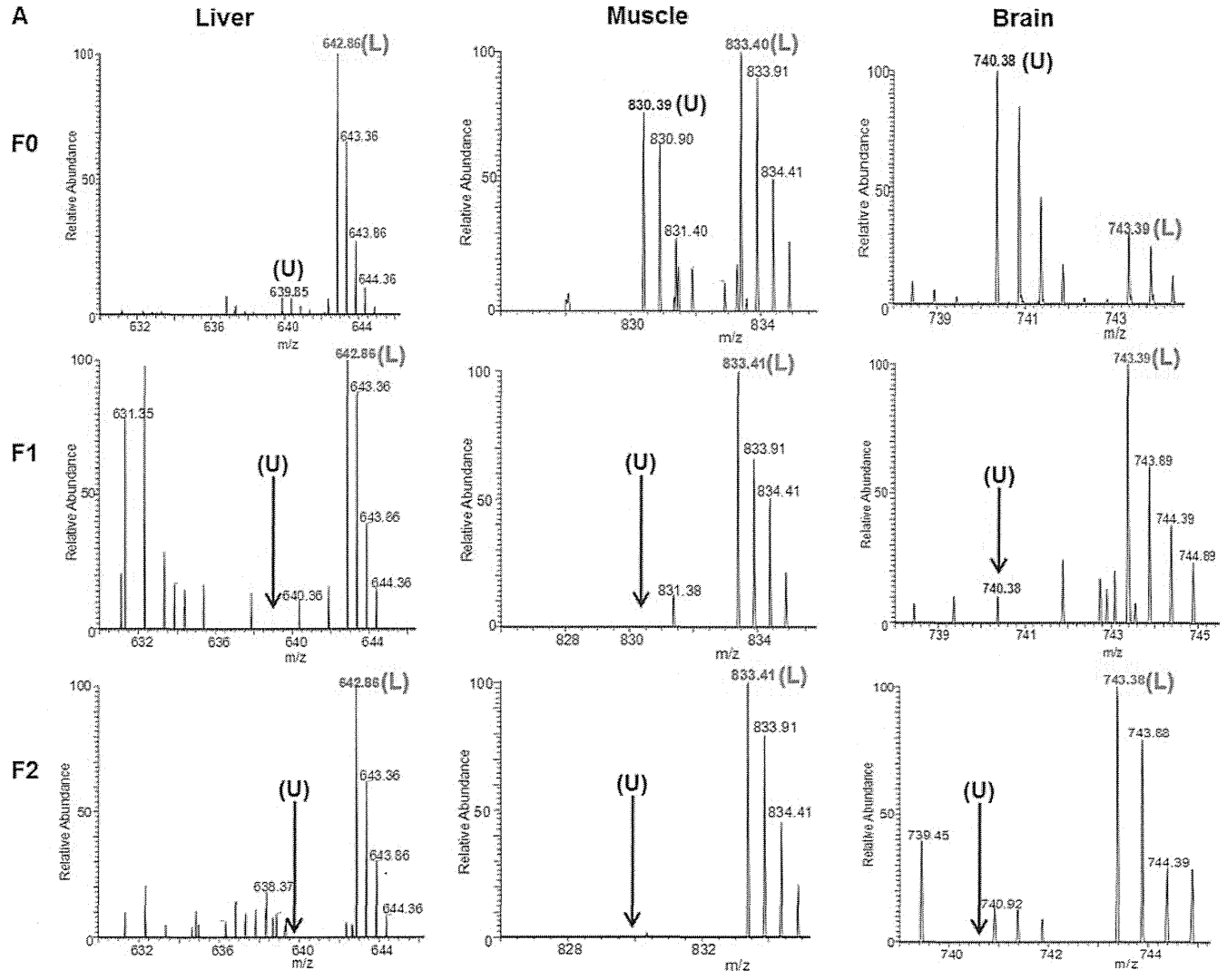

FIG. 1A. **$^{13}C_6$-lysine labeling efficiency in various tissues.** *A*, an example of spectra for labeled (L) and unlabeled (U) peptide pairs is shown for the same peptide sequence of the same protein in each tissue across the F0, F1, and F2 generations. The "Liver" panel shows doubly charged ions at *m/z* 639.85 and 642.86 for unlabeled and labeled peptide (TLGVDFIDVATK) for carbamoyl phosphate synthase, a liver-specific protein. The "Muscle" panel shows doubly charged ions at *m/z* 830.39 and 833.40 for unlabeled and labeled peptide (QAEEAEEQSNVNLAK) for myosin-4, a muscle-specific protein. The "Brain" panel shows doubly charged ions at *m/z* 740.38 and 743.39 for unlabeled and labeled peptide (MYGVLPWNAFPGK) for the myelin proteolipid protein, a brain-specific protein.

assay buffer (100 mM Tris, pH 8.0, 2 mM EDTA, 1.25 mM L-malate, 0.25 mM NAD), 0.01% Triton X-100 (v/v), and 6 U/ml malate dehydrogenase (Sigma) to monitor the enzyme activity. The production of $NADH,H^+$ was recorded after the addition of 5 μl acetyl-CoA (50 μM). Enzyme activities were fluorometrically measured (excitation, λ 340 nm; emission, λ 450 nm) and represented as the mean ± S.E.

Immunohistochemical Staining—Frozen human muscle biopsies of mutation-defined dystrophin-deficient (DMD) (n = 3) and control (normal) (n = 3) tissues were obtained without any identifiers (IRB Protocol No. 2405). Muscle tissues were sectioned and immunostained using rabbit anti-vimentin (Epitomics) and mouse anti-ILK antibodies (Santa Cruz) and HRP-conjugated anti-rabbit or anti-mouse (Dako, Carpinteria, CA) as the primary and secondary antibodies, respectively. As a specificity control, other serial sections were stained with secondary antibody alone.

For all validation assays, the statistical significance between mdx and C57BL/6 parameters was determined using Student's t test. For all measurements, $p < 0.05$ was considered a statistically significant difference.

RESULTS

The incorporation of $^{13}C_6$-lysine Complete by F2 Generation—The efficiency of $^{13}C_6$-Lys incorporation was monitored in the liver, brain, and muscle tissue of generations F0, F1, and F2. Mice fed with the custom diet showed progressive incorporation of the ^{13}C-Lys into the proteins of different tissues at each generation (Figs. 1*A* and 1*B*). Most proteins were fully labeled (labeling efficiency ≥ 96%) in the liver, muscle, and brain by the F2 generation (Fig. 1*B*). Liver proteins showed the fastest incorporation rates for heavy lysine, as the relative abundance of heavy peptide was higher even at

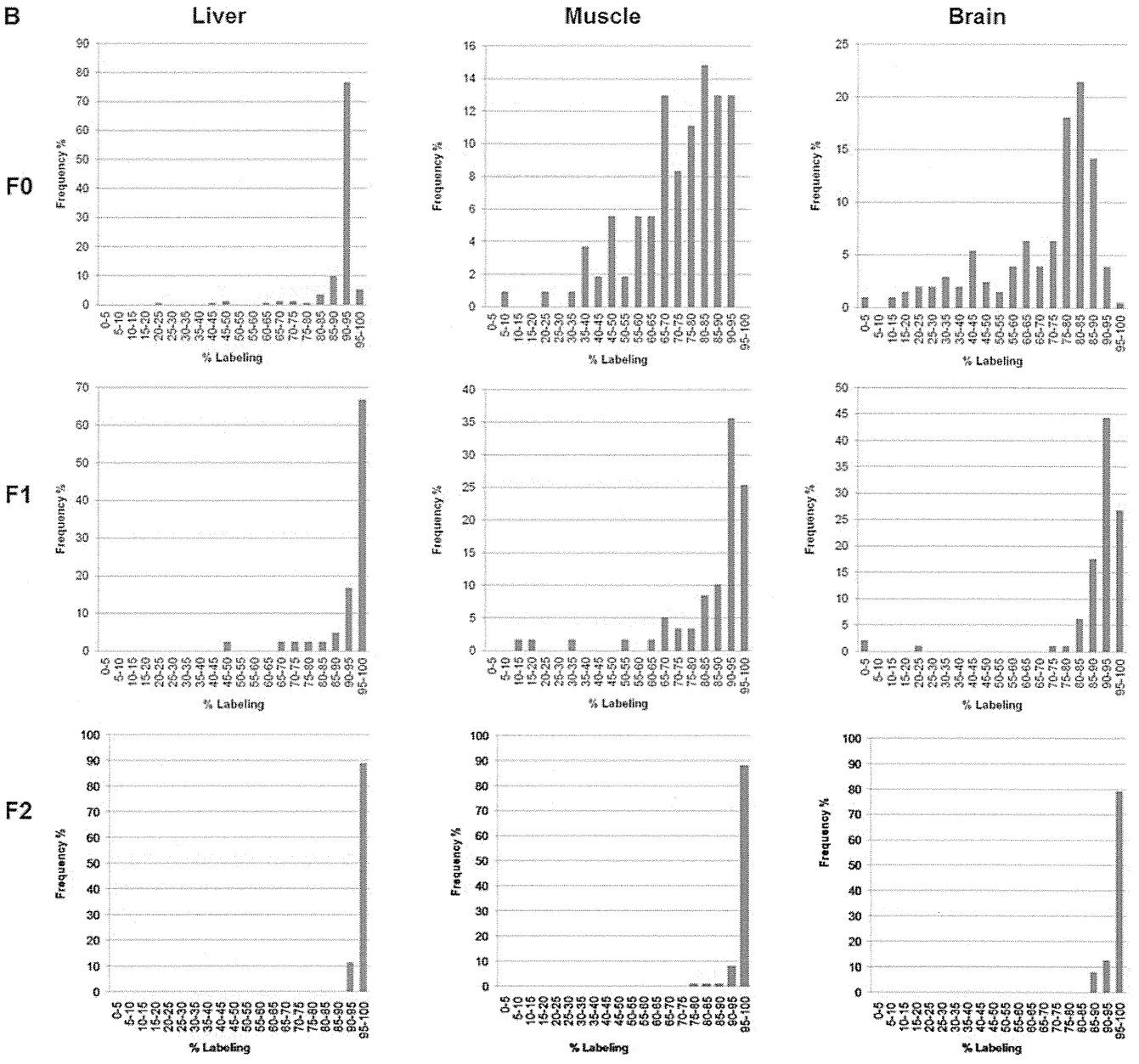

FIG. 1B—*continued B*, overall labeling efficiency of several proteins identified in liver, muscle, and brain tissues across the F0, F1, and F2 generations for SILAC mice.

F0 (Fig. 1*A*, liver). In contrast, brain and muscle tissues showed slower incorporation rates (Fig. 1*A*). By F2 generation, the percent labeling efficiency (mean ± S.E.) by heavy lysine was 97.88 ± 0.38, 96.50 ± 0.95, and 98.26 ± 0.38 in liver, brain, and muscle tissues, respectively. Furthermore, we found that the heavy-lysine diet did not affect the overall health of the C57BL/6 mice, including with regard to their body weight and fertility.

Differential Protein Expression in the Gastrocnemius of Dystrophin-deficient mdx Mice Relative to Age-matched C57BL/6 Controls—Signs of muscle necrosis start at about 3 weeks of age in mdx mice; therefore, we investigated the skeletal muscle proteome at this early stage. We performed differential proteome profiling of the skeletal muscle in pairs of SILAC-labeled-C57BL/6 and unlabeled-C57BL/6 mice and pairs of SILAC-labeled C57BL/6 and unlabeled dystrophic mdx mice. The control experiment showed a narrower distribution of unlabeled-to-labeled protein ratios, with an average mean ± S.D. of 0.96 ± 0.5, indicating that there were fewer differences in the skeletal muscle proteome between the two wild-type mice examined (Fig. 2; supplemental Tables S1 and S2). In contrast, the comparison of unlabeled mdx and SILAC-labeled C57BL/6 mice showed a wider distribution of protein ratios, with an average mean ± S.D. of 1.52 ± 1.3, indicating

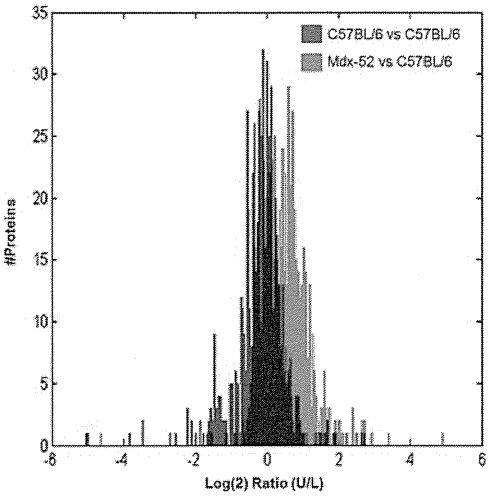

FIG. 2. **Distribution profiles of unlabeled-to-labeled protein ratios.** Gastrocnemius muscle was harvested from SILAC-labeled C57BL/6 mice (F2 generation) and from age-matched unlabeled mdx-52 and unlabeled C57BL/6 mice. SILAC ratios obtained for unlabeled C57BL/6 *versus* labeled C57BL/6 (blue) and unlabeled mdx *versus* labeled C57BL/6 (red) were transformed to log values and plotted. An overlay for these plots shows the distribution profiles. Ratios of unlabeled to labeled peptide pairs were obtained using IP2 software. The overall mean ± S.D. was 1.52 ± 1.3 for unlabeled mdx *versus* labeled C57BL/6 and 0.96 ± 0.5 for the unlabeled *versus* labeled C57BL/6 mice.

that there are several proteins whose relative abundances are significantly altered in the skeletal muscle proteome of mdx mice relative to C57BL/6 control mice (Fig. 2).

Furthermore, Figs. 3*A* and 3*B* show a representative mass spectrum and extracted ion chromatogram for a peptide belonging to dystrophin protein that is completely absent from mdx muscle but present in C57BL/6 muscle. Figs. 3*E* and 3*F* show data for a peptide of talin-1 that was significantly up-regulated in mdx muscle relative to C57BL/6 muscle. In contrast, Figs. 3*C* and 3*D* show data for glyceraldehyde phosphate dehydrogenase protein, which remained unchanged between mdx and C57BL/6 muscle. Taken together, these data indicate that the SILAC strategy can efficiently detect specific protein alterations in dystrophin-deficient skeletal muscle relative to normal skeletal muscle.

Differentially Altered Proteins and Pathways Identified in Dystrophin-deficient Muscle—In the initial proteomic analysis, 750 to 850 proteins (with ≥2 unique peptides) were identified and quantified in gastrocnemius muscle. Among these, ~250 proteins were found to be differentially altered in their levels by at least a factor of ±1.5 in mdx muscle relative to C57BL6 control muscle. These proteins mainly belonged to the muscle cytoskeleton, mitochondrial energy metabolism, glycolysis, citric acid cycle, sarcoplasmic reticulum, and calcium homeostasis pathways. Further, to validate the initial proteomic data, we used a spike-in strategy in an independent set of mdx mice (n = 3) and C57BL/6 control mice (n = 3) that were maintained on regular feed. These analyses identified ~75 proteins whose abundance was significantly altered ($p < 0.05$) between the mdx and wild-type mice (Table I; supplemental Table S3). Proteins such as vimentin, annexin-2, and desmin were found to be up-regulated (>2.5-fold) in the muscle of mdx mice relative to C57BL/6 mice, whereas proteins such as myosin and tropomyosin were found to be significantly down-regulated (−2.0-fold) in mdx relative to C57BL/6 muscle (Table I). IPA of the proteome profiling data revealed significant ($p < 0.05$) alterations in mitochondrial function, energy metabolism (citrate cycle, glycolysis), actin cytoskeleton signaling, and ILK pathways in dystrophin-deficient skeletal muscle, indicating their potential role in early dystrophic pathology (supplemental Fig. S1).

The ILK Pathway Is Up-regulated in Dystrophin-deficient Muscle—Once differential SILAC proteome profiling and IPA identified the involvement of the actin cytoskeleton and ILK pathways in dystrophin-deficient muscle pathology, we sought to validate these findings using independent assays and an independent set of mice that were maintained on regular mouse feed. Proteins involved in this pathway and those that were found to be differentially altered in our proteome profiling experiments, such as vimentin, desmin, and annexin-2, were validated by means of immunoblotting. As expected, these proteins were found to be significantly up-regulated ($p < 0.05$) in dystrophin-deficient muscle relative to C57BL/6 muscle (Figs. 4*A*, 4*B*, 4*D*, and 4*E*). These results are in agreement with the SILAC proteome profiling data. Furthermore, we validated the significant up-regulation of ILK itself in dystrophin-deficient muscle, even though we did not detect this protein in our profiling studies (Figs. 4*A*, 4*C*). In addition, the presence of additional coordinate players of the actin cytoskeletal and integrin linked pathways, such as cofilin and profilin, was examined in dystrophin-deficient muscle via immunoblot analysis (supplemental Fig. S2). Profilin showed a 1.6-fold up-regulation in the proteomic analysis, but immunoblotting showed no difference between mdx and C57BL/6 muscle. In sum, these results indicate that proteins involved in the actin cytoskeletal and ILK pathways are up-regulated in dystrophin-deficient muscle, indicating their potential role in disease pathology.

Vimentin and ILK Are Elevated in Human DMD Muscle Biopsies—Immunostaining was performed in normal and DMD muscle tissues to validate the data obtained in the mdx mouse model. This analysis revealed increased staining for vimentin and ILK in the muscle biopsies of DMD patients relative to normal tissues (Fig. 5). In the normal skeletal muscle, the vimentin staining was predominantly observed in capillaries; however, in the dystrophic muscle, striking vimentin staining was observed in the capillaries and muscle infiltrates, including staining in some myofibers (Figs. 5*A*, 5*B*). ILK staining was observed in the capillaries of normal skeletal muscle; however, in dystrophic muscle, ILK staining was striking in both the blood vessels and the myofibers (Figs. 5*C*–5*E*). These results indicate that the altered pathways identified in

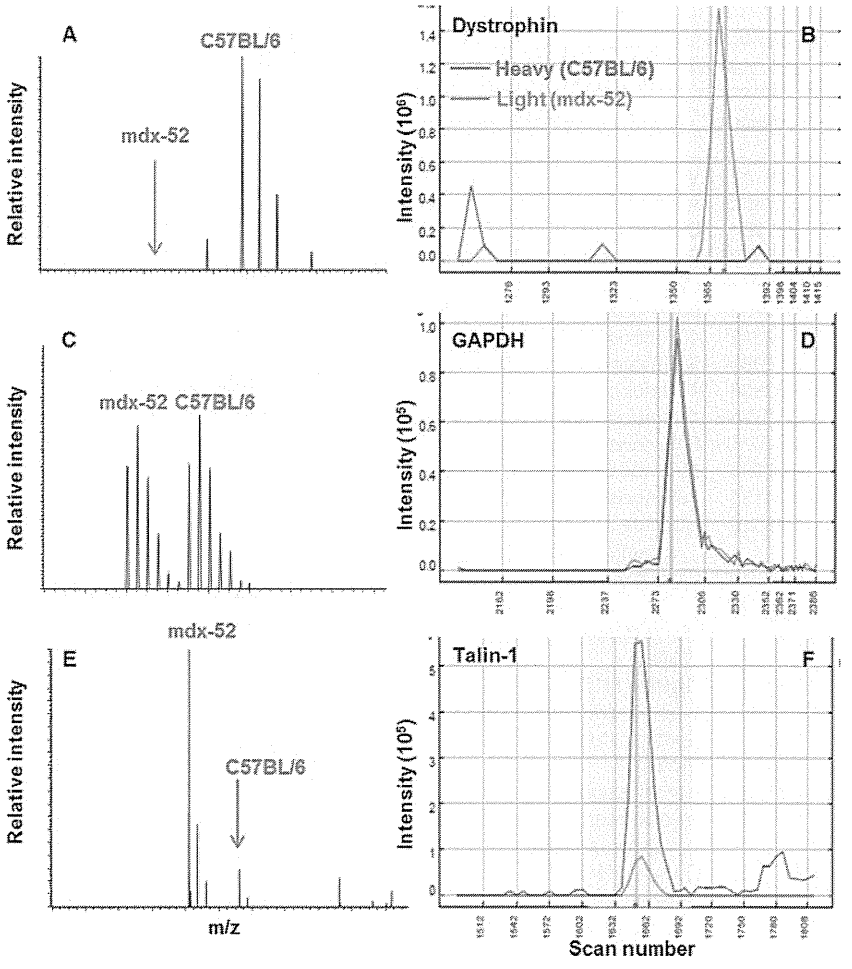

FIG. 3. **MS spectra of selected proteins with differential modulation in dystrophin-deficient muscle.** Gastrocnemius muscle was obtained from SILAC-labeled C57BL/6 and unlabeled mdx-52 mice, and MS analysis was performed. *A*, *B*, a representative mass spectrum for labeled and unlabeled peptide of dystrophin protein and its elution profile, indicating a complete absence of dystrophin peptide in mdx mice. *C*, *D*, a representative mass spectrum for labeled and unlabeled peptide of glyceraldehyde 3 phosphate dehydrogenase (GAPDH) and its elution profile, indicating no change in its level between C57BL/6 and mdx mice. *E*, *F*, a representative mass spectrum for labeled and unlabeled peptide of talin-1 protein, indicating its up-regulation in mdx relative to C57BL/6 mice. All peptide ions shown were detected as doubly charged species at their respective *m/z* values, with a mass error < 10 ppm.

the muscle of mdx mice are also perturbed in the muscle of human DMD patients.

Mitochondria and Metabolic Enzymes Are Affected in Dystrophin-deficient Muscle—Differential SILAC proteome profiling identified various mitochondrial and metabolic enzymes, including hydroxyacyl-coenzyme A dehydrogenase, trifunctional enzyme subunit beta, aconitate hydratase, isocitrate dehydrogenase [NAD] subunit α, and lactate dehydrogenase, as down-regulated in dystrophin-deficient muscle (Table I). Further IPA analyses of the data pointed to mitochondrial and metabolic dysfunction in dystrophin-deficient muscle; we sought to validate these findings by means of independent biochemical assays. The activities of two mitochondrial respiratory chain enzymes (lactate dehydrogenase and citrate synthetase) were monitored in normal and dystrophin-deficient muscle (Fig. 6). Dystrophin-deficient muscle showed a significant decrease (−2-fold) ($p < 0.05$) in lactate dehydrogenase activity relative to C57BL/6 muscle ($p < 0.05$). In contrast, no difference was observed in citrate synthase activity between the dystrophic and C57BL/6 muscle (data not shown). Interestingly, no difference was observed in the levels of other mitochondrial proteins, including cytochrome *c* and transcription factor A mitochondrial, monitored via immunoblotting analysis of dystrophin-deficient and normal muscle (data not shown). In sum, these results indicate that there might be subtle differences in some of the mitochondrial respiratory chain enzymes between mdx and C57BL/6 mice that cannot be detected via immunoblotting but which can be detected with the use of a sensitive proteome profiling method employing a stable isotope labeling strategy.

DISCUSSION

Initially, proteome profiling using the SILAC strategy could be implemented only in *in vitro* cell-culture-based systems or, to some extent, *in vivo* using nematodes and drosophila (13, 17, 27, 28). More recently, this versatile technique has been extended to the metabolic labeling of whole mammals with stable isotopes using either $^{13}C_6$-Lys-supplemented feed (SILAC mouse) or ^{15}N-supplemented feed (SILAM). These strategies have allowed accurate proteome profiling of tissues and organs in *in vivo* systems under different physiological conditions (18, 19). In the current study, we extended the application of the SILAC mouse strategy to obtain insights into proteomic alterations in dystrophin-deficient skeletal muscle at the early stage of the pathology. Examination of the gastrocnemius muscle of dystrophic mdx mice at the early

TABLE I
Significantly modulated proteins in gastrocnemius muscle of 3-week-old dystrophin deficient mdx mice relative to C57BL/6 mice

Accession[a]	Protein name[b]	Fold change[c]
P20152	Vimentin	3.51
P07356	Annexin A2	3.18
P31001	Desmin	2.69
Q6ZWV3	60S ribosomal protein L10	2.46
P35979	60S ribosomal protein L12	2.25
P19253	60S ribosomal protein L13a	2.18
P62242	40S ribosomal protein S8	2.09
P35980	60S ribosomal protein L18	2.03
P62908	40S ribosomal protein S3	2.02
Q6ZWN5	40S ribosomal protein S9	1.99
Q9CXW4	60S ribosomal protein L11	1.99
P67984	60S ribosomal protein L22	1.96
P14131	40S ribosomal protein S16	1.95
P68040	Guanine nucleotide-binding protein subunit beta-2-like 1	1.94
Q8BTM8	Filamin-A	1.88
O88990	Alpha-actinin-3	1.79
Q9JI91	Alpha-actinin-2	1.79
P26039	Talin-1	1.77
P15864	Histone H1.2	1.77
Q00897	Alpha-1-antitrypsin 1–4	1.74
Q921I1	Serotransferrin	1.71
P62962	Profilin-1	1.65
P07724	Serum albumin	1.64
P97457	Myosin regulatory light chain 2, skeletal muscle isoform	1.64
P01027	Complement C3	1.61
P14824	Annexin A6	1.55
P99024	Tubulin beta-5 chain	1.52
P68372	Tubulin beta-2C chain	1.47
P20029	78 kDa glucose-regulated protein	1.46
Q9ERD7	Tubulin beta-3 chain	1.43
Q9JK37	Myozenin-1	1.42
Q8VHX6	Filamin-C	1.42
P48036	Annexin A5	1.39
Q99PT1	Rho GDP-dissociation inhibitor 1	1.38
P23953	Liver carboxylesterase N	1.36
Q62234	Myomesin-1	1.29
P63101	14–3-3 protein zeta/delta	1.28
Q9CQZ5	NADH dehydrogenase (ubiquinone) 1α subcomplex subunit 6	1.25
Q3V1D3	AMP deaminase 1	1.25
Q8QZY1	Eukaryotic translation initiation factor 3 subunit L	1.23
Q9ERS2	NADH dehydrogenase (ubiquinone) 1α subcomplex subunit 13	1.22
Q9WUB3	Glycogen phosphorylase, muscle form	1.21
P20108	Thioredoxin-dependent peroxide reductase, mitochondrial	1.18
P99029	Peroxiredoxin-5, mitochondrial	1.17
Q64727	Vinculin	1.17
Q9D051	Pyruvate dehydrogenase E1 component subunit β mitochondrial	1.07
Q9D6R2	Isocitrate dehydrogenase (NAD) subunit α, mitochondrial	−1.12
Q99KI0	Aconitate hydratase, mitochondrial	−1.12
P47934	Carnitine O-acetyltransferase	−1.15
P48962	ADP/ATP translocase 1	−1.17
Q9WUZ7	SH3 domain-binding glutamic acid-rich protein	−1.17
O55126	Protein NipSnap homolog 2	−1.18
P32848	Parvalbumin alpha	−1.18
P41216	Long-chain-fatty-acid–CoA ligase 1	−1.19
Q61425	Hydroxyacyl-coenzyme A dehydrogenase, mitochondrial	−1.21
Q6P8J7	Creatine kinase, sarcomeric mitochondrial	−1.23
Q99JY0	Trifunctional enzyme subunit beta, mitochondrial	−1.23
P51174	Long-chain specific acyl-CoA dehydrogenase, mitochondrial	−1.24
Q8BMS1	Trifunctional enzyme subunit alpha, mitochondrial	−1.25
P42125	3,2-trans-enoyl-CoA isomerase, mitochondrial	−1.27
P05201	Aspartate aminotransferase, cytoplasmic	−1.29
P13412	Troponin I, fast skeletal muscle	−1.35
P16125	L-lactate dehydrogenase B chain	−1.36
P11404	Fatty acid-binding protein, heart	−1.38
A2ASS6	Titin	−1.43
P68033	Actin, alpha cardiac muscle 1	−1.64
P68134	Actin, alpha skeletal muscle	−1.65
P13541	Myosin-3	−1.71
P13542	Myosin-8	−1.83
Q5SX40	Myosin-1	−1.86
Q5SX39	Myosin-4	−2.12
P58771	Tropomyosin alpha-1 chain	−2.33
P58774	Tropomyosin beta chain	−2.63

[a] Accession numbers are from the Uniprot database.
[b] Protein names are from the Uniprot database; significantly different protein modulations ($p < 0.05$) were determined using the non-parametric Wilcoxson rank sum test.
[c] Fold changes were calculated using mdx/wt (unlabeled/labeled) ratios quantitated using Integrated Proteomics Pipeline software. Ratios were obtained from $n = 3$ mice/group.

stage of disease showed significant alterations in its proteome. Altered pathways included ILK, actin cytoskeleton signaling, mitochondrial energy metabolism, and calcium homeostasis. Some of these pathways were further validated in a separate group of mdx mice, as well as in human DMD biopsies.

Feeding C57BL/6 (normal) mice with a synthetic diet supplemented with $^{13}C_6$-Lys (heavy) did not affect their growth or reproductive parameters, even after a prolonged feeding period, over a course of two generations. These observations are in accordance with the results of an earlier study using this diet (18). The labeling efficiency in different organs and tissues, including liver, muscle, and brain, by the heavy lysine reached a maximum by the F2 generation. Of the three tissue types, liver had the fastest incorporation rate (≥70% of its proteins were 90% to 95% labeled with heavy lysine at about 50 days of feeding in the F0 generation); this is probably due to the rapid protein turnover in the liver. In contrast, terminally

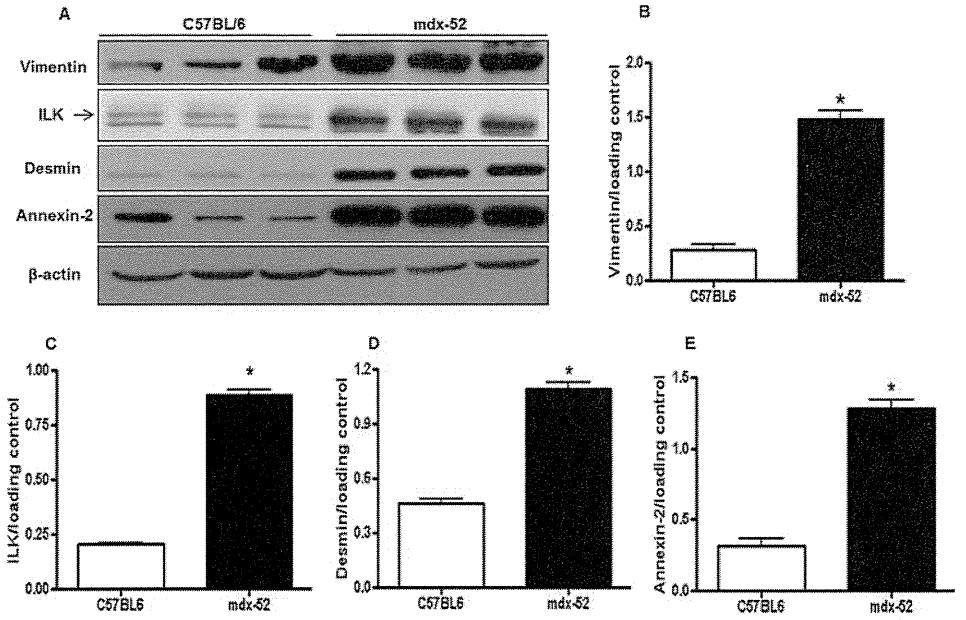

FIG. 4. **Up-regulation of actin cytoskeletal and integrin-linked kinase (ILK) pathways in dystrophic muscle.** *A*, gastrocnemius muscle lysates from C57BL/6 and mdx-52 mice (n = 3/group) were obtained, and homogenates were immunoblotted with antibodies against vimentin, ILK, desmin, and annexin 2. Equal amounts of the protein were electrophoresed in each gel lane, and representative immunoblots are shown. β-actin was used as a loading control. The ratios of respective proteins to β-actin were calculated via densitometric analysis using Quantity One software, and the data are represented as means ± S.E. *B–E*, quantifications for the respective proteins (*$p < 0.05$).

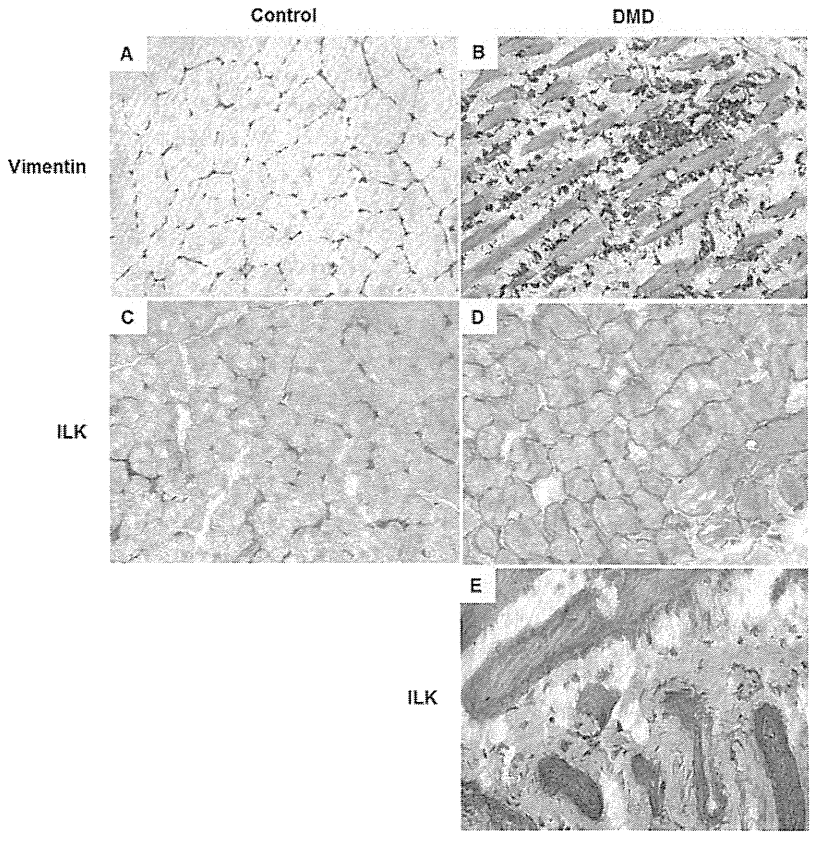

FIG. 5. **DMD patient muscle biopsies showing enhanced vimentin and ILK expression.** Frozen sections (n = 3/group) of DMD and control human muscle biopsies were stained with rabbit anti-vimentin and mouse anti-ILK antibodies. Anti-rabbit and anti-mouse horseradish peroxidases were used as secondary antibodies, respectively. Representative pictures are shown for vimentin (*A*, *B*) and ILK (*C–E*) for normal (*A*, *C*) and DMD (*B*, *D*, *E*) muscles biopsies (20×).

differentiated tissues such as muscle and brain incorporated heavy lysine at a slower rate, as indicated by the wider distribution of labeling percentages in the F0 and F1 generations. These results suggest that proteomic profiling studies involving muscle need to use tissues from mice fed with a heavy-lysine diet at least for two generations. The overall labeling